Carbohydrate Polymers 83 (2011) 94–115

Contents lists available at ScienceDirect

Carbohydrate Polymers

journal homepage: www.elsevier.com/locate/carbpol

Utilization of carboxymethyl cellulose based on bean hulls as chelating agent. Synthesis, characterization and biological activity

Atef A. Ibrahim [a], Abeer M. Adel [a], Zeinab H. Abd El–Wahab [b,*], Mona T. Al–Shemy [a]

[a] Cellulose and Paper Department, National Research Center, Dokki, Cairo, Egypt
[b] Chemistry Department, Faculty of Science (Girl's), Al-Azhar University, Nasr City, P.O. Box 11754, Cairo, Egypt

ARTICLE INFO

Article history:
Received 28 June 2010
Received in revised form 9 July 2010
Accepted 12 July 2010
Available online 17 July 2010

Keywords:
Carboxymethyl cellulose
Polymeric binary and ternary metal complexes
Electronic spectra and biological study

ABSTRACT

Binary and ternary complexes of Ni^{2+}, Cu^{2+}, Ag^{+} and UO_2^{2+} with the prepared carboxymethyl cellulose in its sodium salt (P-NaCMC) and pyridine (py) as secondary ligand have been prepared. Probable structures of the binary and ternary complexes were inferred via elemental analysis, spectral data (IR, mass and solid reflectance) as well as magnetic susceptibility measurements, thermal and XRPD analysis. The change in the selected vibrational absorption bands in IR spectrum of P-NaCMC upon coordination with metal ions investigates the coordination mode of P-NaCMC to be the two vicinal uncarboxylated diol groups (2- and 3-hydroxyl groups) of the glucopyranose rings in addition to the carbonyl oxygen atom of the carboxylate group while the coordination mode of pyridine ligand is the ring nitrogen. The mass spectra confirmed the proposed structure of the synthesized compounds. The solid reflectance spectral data and magnetic moment measurements suggest the geometrical structures for the metal complexes. Thermal studies suggest a mechanism for degradation of P-NaCMC and its metal complexes as function of temperature supporting the chelation modes. Also, the activation thermodynamic parameters, such as, ΔE^*, ΔH^*, ΔS^* and ΔG^* for the different thermal decomposition steps of P-NaCMC and its metal complexes were calculated. Antimicrobial activities of P-NaCMC and its binary and ternary complexes were studied against *S. aureus* and *S. pyogenes* (Gram-positive bacteria), *P. phaseolicola* and *P. fluorescens* (Gram-negative bacteria) and the fungi; *F. oxysporum* and *A. fumigates* using agar disc diffusion method. The results showed that all the metal complexes, especially Cu^{2+} ternary complex have higher antibacterial and antifungal activities than P-NaCMC.

1. Introduction

Polymers are defined as molecules with high molecular weight formed by the repetition of monomeric units linked with covalent bonds. In comparison, coordination polymers are infinite systems build up with metal ions and organic ligands as the main elementary units that are linked via coordination bonds and other weak chemical interactions. These compounds are also named metal–organic coordination networks or metal–organic frameworks (MOF) (Çolak, Yeşilel, & Büyükgüngör, 2010). The synthesis of coordination polymers is usually achieved by one of the following procedures: (i) metal complexes may yield polymeric material during their formation because of the presence of favourable donor groups in the ligand. (ii) The ligand itself may act as an organic polymer to which metals can be suitably coordinated. (iii) A metal ion may be coordinated with a ligand and the monomeric metal complex may react with another organic compound to form polymeric complexes (Nishat, Ahmad, & Ahamad, 2006; Sacarescu, Ardeleanu, Sacarescu, Simionescu, & Mangalagiu, 2007).

Cellulose is one of the most abundant naturally occurring biopolymer and it is commonly found in the cell walls of plants and certain algae. Cellulose has three reactive hydroxyl groups per anhydroglucose repeating unit that form inter- and intramolecular hydrogen bonds. These bonds strongly influence the chemical reactivity and solubility of cellulose (Dahou, Ghemati, Oudia, & Aliouche, 2010; Sundar, Sain, & Oksman, 2010; Wada, Ike, & Tokuyasu, 2010). When transition metal salts are reacted with cellulose, they form coordination bonds with functional groups at the 6th, 2nd and 3rd carbon positions of cellulose, moreover cellulose-based metal complexes have attracted scientists due to its specific applications as in drug delivery systems (Sundar et al., 2010). Many attempts have been made to utilize cellulose as a metal scavenger through some derivatizations. Some of these attempts are based on the introduction of groups with capacity chelating as carboxylate and amine groups (Gurgel, Júnior, Gil, & Gil, 2008). Generally, interactions between heavy metal ions and cellulose or its derivatives can occur in four main ways: (i) intercalation into the cellulose matrix, (ii) adsorption onto the cellulose fibres, (iii) formation of the

* Corresponding author.
E-mail address: zhabdelwahab@yahoo.com (Z.H.A. El–Wahab).

0144-8617/$ – see front matter © 2010 Elsevier Ltd. All rights reserved.
doi:10.1016/j.carbpol.2010.07.026

chemical bonds with the reactive groups of cellulose and (iv) formation of complexes with dissolved cellulose degradation products (Norkus, Vaičiūnienė, Vuorinen, & Macalady, 2004).

In our work, the binary and ternary complexes of Ni^{2+}, Cu^{2+}, Ag^{+} and $UO_2{}^{2+}$ With carboxymethyl cellulose in its sodium salt (P-NaCMC) and pyridine (py) as secondary ligand have been prepared. Probable structures of the binary and ternary complexes were elucidated and confirmed using various spectrometric techniques as elemental analysis, spectral data (IR, mass and solid reflectance) as well as magnetic susceptibility measurements, thermal and XRPD analysis. Moreover, evaluation of the antimicrobial activity of the synthesized compounds was done against *Staphylococcus aureus*, *Streptococcus pyogenes*, *Pseudomonas phaseolicola*, *Pseudomonas fluorescens* and *Fusarium oxysporum* using the agar disc diffusion method (Uruş, Serindağ, & Diğrak, 2005).

Although a survey of the literature reveals that a number of cellulose biomass from various sources has been used as a base material for production of carboxymethyl cellulose (CMC) (Barba, Montané, Rinaudo, & Farriol, 2002a; Barba, Montané, Farriol, Desbrières, & Rinaudo, 2002b; Bono et al., 2009; Toğrul & Arslan, 2003; Yaşar, Toğrul, & Arslan, 2007), the authors are not aware of any previous publication concerning preparation of CMC from bean hulls (BH). So the main objective of this work reported here is to increase the utilization of BH as a base material for production of CMC in addition to investigate the coordination behavior towards some selected metal ions as, Ni^{2+}, Cu^{2+}, Ag^{+} and $UO_2{}^{2+}$.

2. Experimental

2.1. Analysis and physical measurements

Nickel chloride hexahydrate ($NiCl_2.6H_2O$), copper chloride dihydrate ($CuCl_2{\cdot}2H_2O$), silver nitrate ($AgNO_3$) and uranyl nitrate hexahydrate $\{UO_2(NO_3)_2{\cdot}6H_2O\}$ (all purchased from BDH or Sigma) were used as received; Solvents; absolute methyl and ethyl alcohol and diethyl ether were purchased from Merck or Sigma. Commercial carboxymethyl cellulose sodium salt (C-NaCMC) (low viscosity), Acetic acid 96% and acetic acid glacial were purchased from Adwic, El-Nasr. Chemical Co., Cairo, Egypt. Sulfuric acid 97% and hydrochloric acid 37% were purchased from Abco Chemie ENG. LTD. Concentrated nitric and perchloric acid was analytical grade and was used as supplied. Chloroacetic acid 97% was purchased from Fluka, Messerschmittstr, Switzerland.

Elemental analysis of carbon, hydrogen and nitrogen were determined using a PerkinElmer 2408 CHN analyzer. Nickel and copper contents were determined by complexometric titrations with standard EDTA solution after decomposing the polymeric metal complex with a mixture of concentrated nitric and perchloric acids while uranium analyses were performed gravimetrically by igniting the solid complexes in a muffle furnace at 800 °C and weighing the residue as U_3O_8. Silver and chloride contents were also determined gravimetrically (Bassett, Denney, Jeffery, & Mendham, 1978; Mostafa & Aicha, 2002). Melting or decomposition points were measured by electronic melting point apparatus: Griffin & George made in Britain. Infrared spectra were recorded over the 4000–400 cm^{-1} range on a Jasco FT/IR, Nicolet and Model 670 by using KBr pellets. Mass spectra were recorded at 70 eV and 300 °C by using Mass spectrometer, JEOL JMS-AX500. The solid reflectance spectra were recorded on UV–vis–NIR Shimadzu 310 PC spectrophotometer. Magnetic susceptibility of the metal complexes were measured by the Gouy method at room temperature using a Johnson Matthey, Alpha products, model MKI magnetic susceptibility balance and the effective magnetic moments were calculated using the relation $\mu_{eff} = 2.828\,(\chi_m{\cdot}T)^{1/2}$ B·M, where χ_m is the molar susceptibility corrected using Pascal's constants for diamagnetism of all atoms in the compounds. PerkinElmer thermal analysis controller AC7/DX TGA7 was used to record simultaneously the TG and DTG curves; the experiments were carried out in dynamic nitrogen atmosphere (20 ml min^{-1}) with a heating rate 10 °C min^{-1} in the temperature range 20–1000 °C using platinum crucibles. X-ray diffractions patterns were obtained using a Brukur D8 Advance X-ray diffractometer (Germany) at ambient temperature. The diffraction patterns were recorded using copper (Kα) Target with a secondary monochromator at 40 kV and 40 mA. The antimicrobial activity of the ligands and their complexes were screened using the agar disc diffusion method (Uruş et al., 2005).

2.2. Synthesis of sodium carboxymethylcellulose

The manufacture of sodium carboxymethylcellulose involves two reaction steps. In the first step, cellulose is treated with NaOH, often in the presence of an inert solvent, which acts both as a swelling agent and as a dilutant and thus facilitates good penetration of NaOH into the cellulose structure. The cellulose-NaOH activation reaction is often referred to as mercerization and it is generally performed at approximately room temperature. The alkali cellulose is accessible and reactive towards monochloracetic acid which is added to the reaction in the second step either as free acid or as its sodium salt, (Stigsson, Kloow, Germgård, & Andersson, 2005).

The reaction between alkali cellulose and the etherification agent in an aqueous system is normally carried out at about 70 °C according to:

$$\underset{\text{Cellulose}}{\text{Cell-OH}} + \underset{\text{Chloroacetic acid}}{\text{ClCH}_2\text{COOH}} + \text{NaOH} + \text{NaOH} \rightarrow$$

$$\underset{\text{sodium carboxymethyl cellulose}}{\text{Cell-OCH}_2\text{COONa}} + \text{NaCl} + \text{H}_2\text{O}$$

At the same time, NaOH reacts with monochloracetic acid to form sodium glycolat and sodium chloride, i.e. in dissolved form, according to

$$\text{ClCH}_2\text{COOH} + \text{NaOH} \rightarrow \underset{\text{sodium Glycolate}}{\text{HOCH}_2\text{COONa}} + \text{NaCl}$$

In a typical procedure, bean hulls were subjected to prehydrolysis treatments with H_2SO_4 (Adel, Abd El–Wahab, Ibrahim, & Al–Shemy, 2010), pulping (Rodríguez, Moral, Serrano, Labidi, & Jiménez, 2008), bleaching (Ohwoavworhua & Adelakun, 2005) and finally hydrolyzed (Ejikeme, 2008; El-Sakhawy & Hassan, 2007) to produce the microcrystalline cellulose. To a suspension of 5 g of this extracted cellulose in 100 ml ethanol, was add 20% NaOH solution drop wise during 30 min and the mixture was left under stirring for 1 h at room temperature, this is the alkalization process. Secondary, 6.5 g of monochloracetic acid was dissolved in 15 ml of ethanol and added drop wise to the mixture during 30 min then the mixture was allowed to react under stirring at 60 °C for 2 h, this is the etherification process. The mixture was then filtered and the solid phase suspended in 150 ml of 70% methanol and neutralized with 90% acetic acid. The suspension was filtered, washed three times with methanol and dried at 60 °C (Ruzene, Goncalves, Teixeira, & Pessoa De Amorim, 2007; Varshney et al., 2006; Vilela et al., 2010).

2.3. Synthesis of polymeric metal complexes

2.3.1. Synthesis of binary complexes

The binary complexes were prepared by the addition of a hot aqueous solution of the appropriate metal chloride or nitrate (0.001 mmol) (0.238 g $NiCl_2{\cdot}6H_2O$), (0.170 g $CuCl_2{\cdot}2H_2O$), (0.170 g $AgNO_3$) or {0.502 g $UO_2(NO_3)_2{\cdot}6H_2O$} to a magnetic stirred and warm aqueous solution of P-NaCMC (0.001 mmol, 0.260 g) in 1:1 mole ratio. The resulting precipitate polymeric metal complex was stirred for 1 h to ensure complete precipitation then filter through

a sintered glass funnel (G_2), washed with bidistilled water several times to remove excess metal salts or P-NaCMC then ethanol and diethyl ether and dried in air at room temperature for several days. The resultant dry compounds were ground to a powder and stored at ambient temperature in vacuo over calcium chloride until used. All the binary complexes are insoluble in common organic solvents like acetone, ethanol, methanol, chloroform, benzene, DMF and DMSO. The yields obtained were in the range between ~71 and 87%.

2.3.2. Synthesis of ternary complexes

The ternary complexes were prepared in a similar way to the previous method except the presence of the secondary ligand; pyridine. In a typical procedure, a hot aqueous solution of the appropriate metal chloride or nitrate (0.001 mmol) (0.238 g $NiCl_2{\cdot}6H_2O$), (0.170 g $CuCl_2{\cdot}2H_2O$), (0.170 g $AgNO_3$) or {0.502 g $UO_2(NO_3)_2{\cdot}6H_2O$} was add drop wise to a magnetic stirred and warm aqueous solution containing a mixture of the P-NaCMC (0.001 mmol, 0.260 g) and pyridine (0.001 mmol, 0.081 ml) in 1:1:1 mole ratio with constant stirring. The resulting precipitate polymeric metal-complex was stirred for 1 h to ensure complete precipitation then filter through a sintered glass funnel (G_2), washed with bidistilled water several times then ethanol and diethyl ether and dried in air at room temperature for several days. The resultant dry compounds were ground to a powder and stored at ambient temperature in vacuo over calcium chloride until used. All the ternary complexes are insoluble in common organic solvents like acetone, ethanol, methanol, chloroform, benzene, DMF and DMSO. The yields obtained were in the range between ~65 and 88%. Unfortunately we were not able to obtained the ternary Ni(II) complex due to formation of hydro gel not solid precipitate.

2.4. Antimicrobial assessments

The agar disc diffusion method was employed for the determination of antimicrobial activity of the synthesized compounds (Uruş et al., 2005). The strains are *S. aureus* and *S. pyogenes* (Gram-positive bacteria), *P. phaseolicola* and *P. fluorescens* (Gram-negative bacteria) and the fungi; *F. oxysporum* and *A. fumigatus*. The antibiotics; *chloramphencol*, *Cephalothin* and *cycloheximide* were used as standard reference of Gram-positive bacteria, Gram-negative bacteria and fungi, respectively. The tested compounds were dissolved in dimethyl formamide, DMF which have no inhibition activity to get concentrations of 1 and 2 mg/ml. In the case of insoluble compounds, the compounds were suspended in DMF and vortexes then processed.

The bacteria were first incubated at 30 ± 0.1 °C for 16 h in nutrient broth medium (Difco). After injecting 0.1 ml cultures of the bacteria into petri dishes (9 cm), 15 ml of Mueller Hinton agar (MHA, sterilized in a flask and cooled to 45–50 °C) were homogeneously distributed onto the sterilized petri dishes. Sterilized blank paper discs (6 mm in diameter) were impregnated by equal volume (10 μl) from the specific concentration of dissolved compounds and carefully placed on surface of each inoculated plate. The plates were then incubated at 37 ± 0.1 °C for 36 h. For antifungal activity, the same method as for bacteria was adopted. Instead of nutrient agar, Potato dextrose agar medium (PDA, 250 g of potato + 20 g of dextrose + 20 g of agar) was used. The inoculated medium was incubated at 25 °C for three days. Four replicates were carried out for each extract against each of the test organism. After incubation, the diameters of the resulted and growth inhibition zones were measured averaged and the mean values recorded in millimeter were tabulated. Additionally, the activity index (%) was calculated (Abd El–Wahab, 2008b; Singh, Singh, & Singh, 2008).

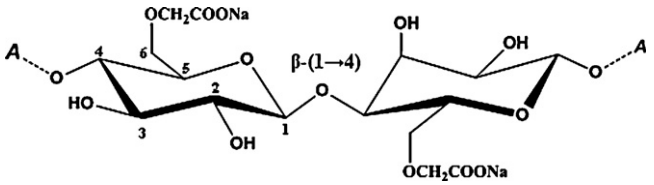

Fig. 1. Structural formula of two adjacent monomeric units of carboxymethylcellulose, sodium salt. *A* represents the continuation of the polymeric chain.

3. Results and discussion

3.1. Charecterization of sodium carboxymethyl cellulose

3.1.1. Determination of degree of substitution

The average degree of substitution (DS) of carboxymethyl cellulose is defined as the average number of carboxymethyl groups per repeating unit and is usually in the range 0.4–1.5 (Du et al., 2009; Kutsenko, Bochek, Vlasova, & Volchek, 2005; Naves & Petri, 2005; Suflet, Chitanu, Valentin, & Popa, 2006). Numerous techniques permit to characterize DS value (Capitani, Porro, & Segre, 2000; Hedlund & Germgård, 2007; Melander & Vourinen, 2001; Oudhoff, Buijtenhuij, Wijnen, Schoenmakers, & Kok, 2004; Peydecastaing, Vaca-Garcia, & Borredon, 2009; Vaca-Garcia, Borredon, & Gaseta, 2001; Yuen, Choi, Phillips, & Maa, 2009). In a typical procedure: To a suspension of 4 g of sample in 75 ml ethanol, was add 5 ml of nitric acid and the mixture was agitated and boil for 5 min followed by further stirring at room temperature for other 10 min. Liquid solution was decanted using a vacuum pump and washed several times with 80% ethanol (60 °C), then the precipitate was washed with anhydrous methanol. Finally, the filter was dried at 105 °C for 3 h to 1–1.5 g of dry P-NaCMC in 100 ml water, was adding 25 ml of sodium hydroxide solution (0.3 N), then the mixture was agitated and heated to boil for 15–20 min to complete solubility. Finally, the mixture was titrated against 0.3 N HCl and the degree of substitution can be calculated (Bono et al., 2009).

In our work, DS value of P-NaCMC was found to be 0.70 indicating that the presence of one carboxymethyl group for each unhydroglucose unit. Consequently the structural formula of two adjacent monomeric units of P-NaCMC can be represented as in Fig. 1.

3.1.2. Determination of moisture content and thermal characterization

The moisture content was done by successive drying of the sample (0.5 ± 0.0001 g) in an oven at 103 ± 2 °C, cooling in a desiccator and weighing until the difference became negligible. Results are expressed as the mean of three paralleled determinations (Ejikeme, 2008). The determination of moisture content of P-NaCMC indicate that the P-NaCMC still contained amounts of water molecules due to its strong hydrophilicity, which can be calculated from the thermal gravimetric analysis and confirmed by mass spectrum study as clear latter.

The thermal characterization of P-NaCMC is given in Fig. 2. It is clear that the curve consists of four stages, the first one at the temperature range 50–78 °C gives a weight loss due to evaporation of moisture that is 7.70% water content (calculated mass loss 6.93%). Also we examined the water content in the commercial sodium carboxymethylcellulose, C-NaCMC with DS of 0.7 and it is about 8.47%, almost the same as that in P-NaCMC. This observed thermal decomposition behavior was agreed to reported results about thermal decomposition of NaCMC with DS of 0.7 (Li, Sun, & Wu, 2009). Additionally, the second step at the temperature range 78–249 °C represents the volatilization of the volatile matter with estimated mass loss of 6.13%. The third stage represents the maximum weight losses as a result of the pyrolysis process. In this stage, the thermal degradation starts at the temperature range 249–370 °C with a

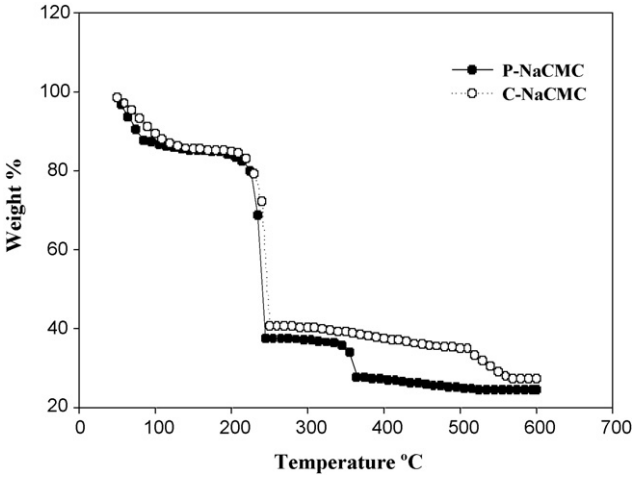

Fig. 2. TGA profile of: P-NaCMC; prepared sodium carboxymethyl cellulose; C-NaCMC; commercial sodium carboxymethyl cellulose.

weight loss of 45.35.The final stage represents the conversion of the remaining material to carbon residues which ends at 561 °C with weight loss of 9.87%. At the end of the combustion process, the residual weight equals to 30.95% compared to 26.92% of C-NaCMC (Franco et al., 2007). The activation energy (ΔE^*), of the various decomposition stages were determined using the Coats–Redfern equation in the following form:

$$\log\left[\frac{\log\{W_f/(W_f-W)\}}{T^2}\right] = \log\left[\frac{AR}{\theta E^*}\left(1-\frac{2RT}{E^*}\right)\right] - \frac{E^*}{2.303RT}$$

where W_f and W are the final and actual weight of the sample, respectively up to temperature T, R is the gas constant, E^* is the activation energy, θ is the heating rate and $(1-(2RT/E)) \approx 1$. Plotting of the left-hand side of this equation against $1/T$, Fig. 3 gives a slope, from the intercept and linear slope of each stage, the (A; the pre-exponential factor) and (ΔE^*) values were determined. The other kinetic parameters; the enthalpy of activation (ΔH^*), the entropy of activation (ΔS^*) and the free energy change of activation (ΔG^*) were calculated using the relationships:

$$\Delta H^* = E^* - RT; \quad \Delta G^* = \Delta H^* - T\Delta S^* \quad \text{and} \quad \Delta S^* = 2.303\left(\log\frac{Ah}{kT}\right)R$$

where (k) and (h) are Boltzman and Planck constants, respectively.

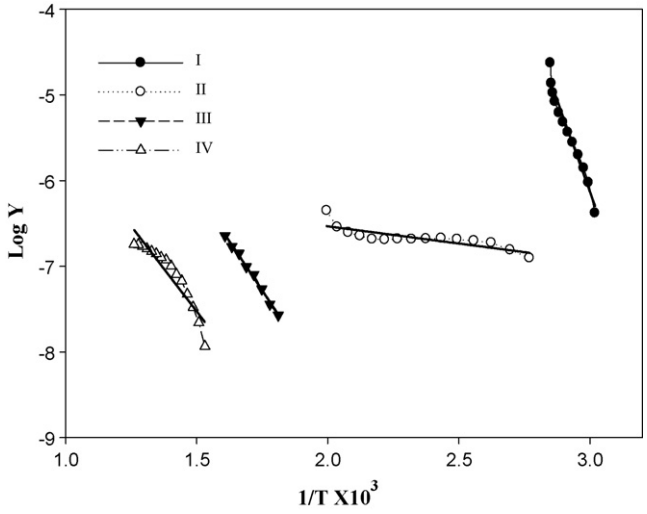

Fig. 3. Coats–Redfern plots of P-NaCMC; prepared sodium carboxymethylcellulose $\log y = \log[\log\{W_f(W_f-W)^{-1}\}T^{-2}]$.

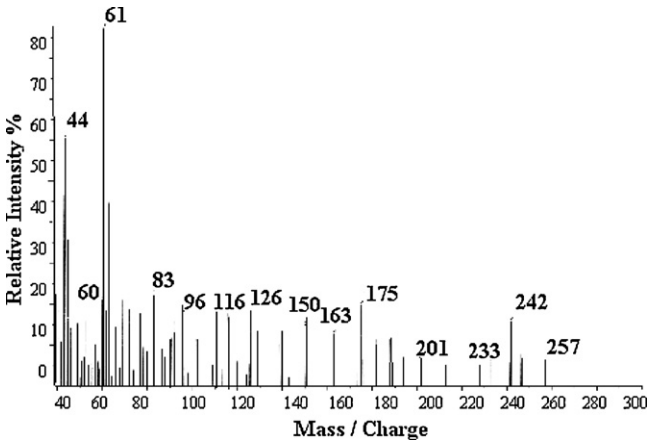

Fig. 4. Mass spectrum of prepared sodium carboxymethyl cellulose, P-NaCMC.

Table 1 presents the characteristic thermal properties and kinetic parameters data based on the weight-loss obtained from the TGA curves for each step in the decomposition sequence of the P-NaCMC under study compared to C-NaCMC.

3.1.3. Elemental analysis and molecular weight determination

The results of elemental analysis of P-NaCMC, Table 2 were in agreement with the suggested formula containing one carboxymethyl group. Additionally, the mass spectrum, Fig. 4 confirms the proposed formula by showing a peak at m/z (%) = 257.00(5.00%) (calcd. 260.20 amu) corresponding to the molecular ion $[M]^+$; $C_8H_{11}O_7Na{\cdot}H_2O$. Fig. 5 shows the suggested mass fragmentation pathway of P-NaCMC.

3.2. Characterization of polymeric metal complexes

3.2.1. Elemental analysis

The results of elemental analysis of metal complexes under study are given in Table 2. The data of elemental analysis are in agreement with 1:1 ligand-to-metal stoichiometry in binary complexes except the silver binary complex, (**3**) in which the ligand-to-metal stoichiometry is 1:2, while, all ternary complexes have the ligands-to-metal stoichiometry are 1:1:1. These data was found to be consistent with the formulae presented in Table 2. The complex formation reactions can be represented as follows:

$$\text{NaCMC} + MCl_2{\cdot}nH_2O \rightarrow [M(CMC)Cl(H_2O)_2]{\cdot}z + A$$

$$M = Ni^{2+};\ n = 6;\ Z = 1.25H_2O;\ A = NaCl + 2.75H_2O$$

$$Cu^{2+};\ n = 2;\ Z = 2H_2O;\ A = NaCl$$

$$\text{NaCMC} + 2AgNO_3/UO_2(NO_3)_2{\cdot}6H_2O \rightarrow [M(CMC_d)X]{\cdot}z + A$$

$$M = 2Ag^+;\ X = 4H_2O;\ Z = 4.5H_2O;\ A = NaNO_3 + HNO_3$$

$$UO_2{}^{2+};\ X = 3H_2O;\ Z = 1.5H_2O;\ A = NaNO_3 + HNO_3 + 1.5H_2O$$

$$\text{NaCMC} + Py + CuCl_2{\cdot}2H_2O \rightarrow [Cu(CMC)(Py)Cl(H_2O)]{\cdot}1.25H_2O + NaCl$$

$$\text{NaCMC} + Py + AgNO_3 \rightarrow [Ag(CMC)(Py)(H_2O)]{\cdot}2.5H_2O + NaNO_3$$

Table 1
Thermal analysis and kinetic parameter data of prepared and commercial carboxymethylcellulose sodium salt.

Sample	Stage	TG range (°C)	DTGA peak (°C)	A (s^{-1})	ΔS^* ($J\,K^{-1}\,mol^{-1}$)	ΔH^* ($kJ\,mol^{-1}$)	ΔG^* ($kJ\,mol^{-1}$)	E^* ($kJ\,mol^{-1}$)
P-NaCMC	I	50–78	64	3.43×10^{22}	0.186	142.266	79.74	145.07
	II	78–249	236	1.77	−0.245	7.321	131.85	11.55
	III	249–370	353	164.22×10^{4}	−0.113	82.576	153.30	87.78
	IV	370–561	528	428.517	−0.203	40.409	202.84	47.07
C-NaCMC	I	50–100	75	1.36×10^{12}	−0.014	73.203	78.049	76.097
	II	100–192	146	67.61×10^{3}	−0.155	29.649	94.73	33.13
	III	192–255	242	3.54×10^{20}	0.144	191.665	117.53	195.95
	IV	255–568	411	18.95×10^{2}	−0.189	42.063	171.42	47.75

P-NaCMC; prepared sodium carboxymethylcellulose; C-NaCMC, commercial sodium carboxymethylcellulose; DTG_{max}, maximum degradation temperature.

Table 2
Analytical data and some physical properties for P-NaCMC ligand and its metal complexes.

Compound no. Empirical formula	M. wt Found (calcd.)[a]	Colour	M.P.$_{de}$ (°C)	Elemental analysis, found (calcd.%)				
				C	H	N	Cl	M
P-NaCMC; $NaC_8H_{11}O_7{\cdot}H_2O$	257.00 (260.20)	White	304	37.11 (36.93)	5.01 (5.05)	–	–	–
(1) $[Ni(CMC)Cl(H_2O)_2]{\cdot}1.25H_2O$; $NiC_8H_{11}O_7Cl{\cdot}3.25H_2O$	373.00 (371.895)	Green	250	25.18 (25.84)	4.80 (4.75)	–	9.50 (9.53)	15.85 (15.78)
(2) $[Cu(CMC)Cl(H_2O)_2]{\cdot}2H_2O$; $Cu\,C_8H_{11}O_7Cl{\cdot}4H_2O$	388.00 (390.27)	Blue	219	25.01 (24.62)	4.66 (4.92)	–	9.10 (9.08)	16.25 (16.28)
(3) $[Ag_2(CMC_d)(H_2O)_4]{\cdot}4.5H_2O$; $Ag_2\,C_8H_{10}O_7{\cdot}8.5H_2O$	586.00 (587.09)	Brown	210	16.94 (16.37)	4.78 (4.64)	–	–	36.69 (36.75)
(4) $[UO_2(CMC_d)(H_2O)_3]{\cdot}1.5H_2O$; $UO_2\,C_8H_{10}O_7{\cdot}4.5\,H_2O$	567.00 (569.30)	Yellow	192	16.19 (16.88)	3.39 (3.37)	–	–	41.03 (41.81)
(5) $[Cu(CMC)(Py)Cl(H_2O)]{\cdot}1.25H_2O$; $Cu\,C_{13}H_{16}O_7NCl{\cdot}2.25H_2O$	436.00 (437.845)	Blue	225	35.29 (35.66)	4.74 (4.68)	3.18 (3.20)	8.41 (8.10)	14.62 (14.51)
(6) $[Ag(CMC)(Py)(H_2O)]{\cdot}2.5H_2O$; $Ag\,C_{13}H_{16}O_7N{\cdot}3.5H_2O$	469.00 (469.24)	Brown	177	33.64 (33.27)	4.96 (4.90)	3.40 (2.99)	–	22.45 (22.99)
(7) $[UO_2(CMC_d)(Py)(H_2O)_2]{\cdot}2.5H_2O$; $UO_2C_{13}H_{15}O_7N{\cdot}4.5H_2O$	648.00 (648.41)	Yellow	222	24.39 (24.08)	3.76 (3.74)	2.13 (2.16)	–	37.54 (36.71)

P-NaCMC, prepared sodium carboxymethyl cellulose ligand; CMC, carboxymethyl cellulose; CMC_d; deprotonated form of carboxymethyl cellulose; Py; pyridine secondary ligand. 1–4, binary complexes; 5–7, ternary complexes.
[a] Found values obtained from mass spectra.

$$NaCMC + Py + UO_2(NO_3)_2{\cdot}6H_2O \rightarrow [UO_2(CMC_d)(H_2O)_2]{\cdot}2.5H_2O + NaNO_3 + HNO_3 + 1.5H_2O$$

3.2.2. IR spectra and mode of bonding in polymeric metal complexes

IR spectra of the microcrystalline cellulose (MCC), prepared sodium carboxymethyl cellulose (P-NaCMC) together with the commercial sodium carboxymethyl cellulose (C-NaCMC) are shown in Fig. 6 and the most important vibrational bands of these samples together with their assignments are given in Table 3.

By comparing the IR spectra of MCC and P-NaCMC, we can observe the appearance of new bands in the spectrum of P-NaCMC at wave numbers of 1613 (ν_{as}) and 1425 cm^{-1} (ν_s) should be assigned to the carboxylic acid salt (COO^-), which confirms that the carboxymethylation has occurred (Adinugraha, Marseno, & H, 2005; Jiang, Li, Zhang, & Wang, 2009; Yang et al., 2010). The broad absorption band at 3420 cm^{-1} for P-NaCMC spectrum was attributed to the stretching vibrations of hydroxyl (OH) groups. These OH groups may include absorbed water and secondary alcohols groups and such broadness may be due to the presence of intramolecular and intermolecular hydrogen bonds (Biswal & Singh, 2004; Kutsenko et al., 2005; Pushpamalar, Langford, Ahmad,

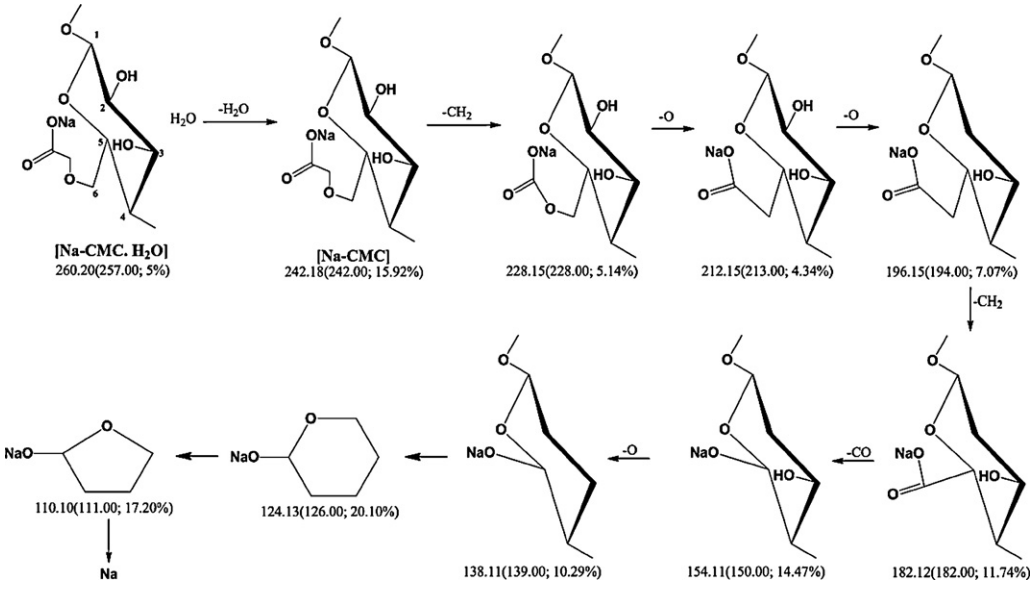

Fig. 5. Suggested fragmentation pathway of P-NaCMC; The values under each fragment denoted as calculated (found; intensity).

Table 3
Main IR spectral vibrations (cm^{-1}) with their assignment for P-NaCMC compared to C-NaCMC and MCC and its metal complexes.

Complex compound	IR spectral vibrations (cm^{-1})							
	ν_{O-H}	ν_{CH}	ν_{COO}	ΔV	ν_{C-O-C}	ν_{M-O}	ν_{M-N}	Additional bands
MCC	3347	2902	–	–	1058	–	–	–
P-NaCMC	3420	2921	1613;1425	188	1059	–	–	–
C-NaCMC	3425	2921	1614;1423	191	1061	–	–	–
(1)	3426	2922	1624;1430	194	1056	599	–	–
(2)	3430	2921	1630;1428	202	1058	482	–	–
(3)	3432	2925	1621;1421	200	1045	580	–	–
(4)	3429	2921	1639;1427	212	1051	578	–	930 (O=U=O)
(5)	3416	2908	1628;1425	203	1061	519	453	1516; 705 (pyridine moiety)
(6)	3412	2902	1599; 1417	182	1058	600	464	1516; 712 (pyridine moiety)
(7)	3437	2922	1631;1426	205	1062	470	432	1576; 712 (pyridine moiety); and 929 (O=U=O)

MCC, microcrystalline cellulose; P-NaCMC, prepared sodium carboxymethyl cellulose; C-NaCMC, commercial sodium carboxymethyl cellulose with a DS of 0.7; 1–4, binary complexes; 5–7, ternary complexes.

& Lim, 2006; Suflet et al., 2006), moreover, the area of these hydroxyl bands is correspondingly smaller than in the spectrum of MCC while, the area of the C=O at 1613 cm^{-1} in the spectrum of P-NaCMC is larger than in the spectrum of MCC due to the esterification process destroyed many intra- and intermolecular hydrogen bonds of cellulose molecules (Chen et al., 2009; Fan, Liu, & Liu, 2010). It is clear that carboxymethyl groups were successfully grafted onto the cellulose skeleton. The IR spectrum of P-NaCMC, also displays a band at 2921 cm^{-1} characteristic of C–H stretching vibrations and corresponded to the aliphatic moieties (Lii, Tomasik, Zaleska, Liaw, & Lai, 2002; Szorcsik, Nagy, Scopelliti, Pellerito, & Sipos, 2006) while, the characteristic bands at 1158 and 1059 cm^{-1} are assigned to C–O–C from the glucosidic units and β-(1 → 4)-glucosidic linkage, respectively (Ma, Xu, Fan, & Liang, 2007; Ren, Sun, & Peng, 2008; Suflet et al., 2006). Examination of IR spectra of the P-NaCMC and C-NaCMC, shows that, the above-mentioned bands of P-NaCMC are also present in commercial C-NaCMC but at slightly different frequencies which gives strong evidence of carboxymethylation process.

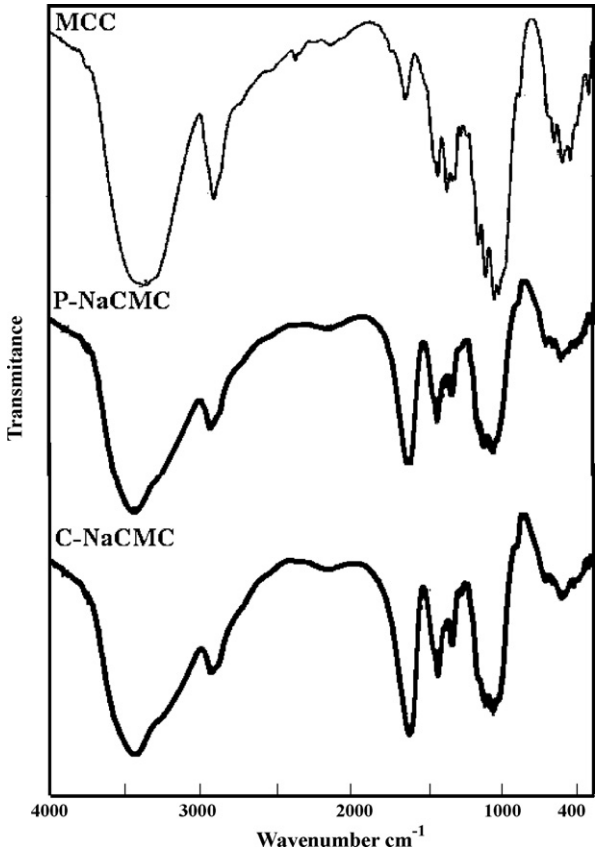

Fig. 6. IR spectra of:
MCC, microcrystalline cellulose
P-NaCMC, prepared sodium carboxymethyl cellulose
C-NaCMC, commercial sodium carboxymethyl cellulose.

Upon comparison between the IR-spectrum of P-NaCMC and those of its metal complexes, binary and ternary, it is clear that the IR spectra of the metal complexes show similar spectral features, although the bands appear at shifted positions and with different intensities. These differences in positions and intensities of the absorption bands are attributed to the formation of the polymeric metal complexes and provide some evidence regarding the bonding sites in the metal complexes. Such comparison brings out the following facts to light:

- The position of the band maxima correspond to stretching vibration of residual uncarboxylated hydroxyl groups are shifted to 3432–3426 and 3437–3412 cm^{-1} in binary and ternary complexes, respectively; this indicates the involvement of a residual hydroxyl group of P-NaCMC in complexation. The presence of a new band in the far IR spectra of all complexes, binary and ternary, in the region 600–470 cm^{-1} ascribable to ν(M–O) support these suggestions (Mashaly, Abd El–Wahab, and Faheim, 2004a; Mashaly, Abd El–Wahab, and Faheim, 2004b).
- With respect to metal–carboxylate interactions, the carboxylate group can coordinate cations in different ways, e.g. ionic (I), monodentate (II), bidentate (III) or bridging (IV) (Papageorgiou et al., 2010) as:

(a) for the bidentate chelating mode

$$\Delta\nu(COO^-)_{complex} << \Delta\nu(COO^-)_{Na\ salt};$$

(b) for bidentate bridging mode

$$\Delta\nu(COO^-)_{complex} \leq \Delta\nu(COO^-)_{Na\ salt};$$

(c) for monodentate geometry of carboxylate group

$$\Delta\nu(COO^-)_{complex} >> \Delta\nu(COO^-)_{Na\ salt};$$

The participation of the carboxylic group in complex formation could be indicated from the changes of the bands of the asymmetric and symmetric stretching vibrations of the ionic carboxylate group upon complex formation. Qualitative pattern of the differences between the wave numbers corresponding to the asymmetric, $\nu_{as}(COO^-)$ and the symmetric, $\nu_s(COO^-)$ stretches of the carboxylate group ($\Delta\nu\,COO^-$) bound with the different cations may be presented as following (Abd El–Wahab, 2007; Filipiuk, Fuks, & Majdan, 2005; Zeleňák, Vargová, & Györyová, 2007):

(a) for the bidentate chelating mode

$$\Delta\upsilon(COO^-)_{complex} \ll \Delta\upsilon(COO^-)_{Na\ \ salt};$$

(b) for bidentate bridging mode

$$\Delta\upsilon(COO^-)_{complex} \leq \Delta\upsilon(COO^-)_{Na\ \ salt};$$

(c) for monodentate geometry of carboxylate group

$$\Delta\upsilon(COO^-)_{complex} \gg \Delta\upsilon(COO^-)_{Na\ \ salt};$$

As can be seen from the experimental data for all metal complexes under study, Table 3 and according to the previous assumptions values of $\Delta\upsilon(COO^-)_{complex}$, it is clear that the mode of the carboxylate binding can be correlated to monodentate mode in all metal complexes except the ternary silver complex, (**6**) which has bidentate character.

- IR spectra of UO_2(II) complexes, (**4**,**7**) display two strong bands at 930 and 929 cm^{-1}, respectively assigned to ν_3(O=U=O) vibration (Abd El–Wahab, Mashaly, Salman, & Faheim, 2004; Abd El–Wahab, Mashaly, & Faheim, 2005; Bontea, Mita, & Humelnicu, 2006; Groenewold, Jong, Oomens, & Stipdonk, 2010). The force constant ($F_{U=O}$) and the bond length (R_{U-O}) were calculated (Abu El-Reash, El-Ayaan, Gabr, & El-Rachawy, 2010; El-Dissouky, El-Bindary, El-Sonbati, & Hilali, 2001; Shoukry & Shoukry, 2008). The calculated bond length values are 7.1405 and 7.1251 mdyn/Å, while the calculated force constant values are 1.7309 and 1.7313 Å for the UO_2(II) complexes, (**4**,**7**), respectively. These values agree well with previously reported values for various uranyl complexes.
- IR-spectra of the ternary complexes, (**5**–**7**) showed two new bands at 1576–1516 and 712-705 cm^{-1} assigned to the pyridine moiety confirmed the participation of pyridine in complex formation via the pyridine nitrogen as previously reported for pyridine complexes (Li, Hu, Xu, & Cai, 2005; Mohamed & Abd El –Wahab, 2005). Moreover, a medium intensity band around 464–432 cm^{-1} assignable for ν(M–N) also supports nitrogen coordination (Abd El–Wahab, 2008a).
- The assignment of the nature of water molecules associated with the complex formation under study was much more complicated as ligand vibrations interfere in this region. The thermal data confirms the nature of water molecule to be lattice/coordinated. The thermal study will be discussed in detailed manner later.
- All the bonding sites participate in the complex formation agree well with previously data reported for similar metal complexes (Ferrari, Grandi, Lazzari, & Saladini, 2005; Filipiuk et al., 2005; Fuks, Filipiuk, & Majdan, 2006; Junicke, Arendt, & Steinborn, 2000; Mukhopadhyay, Kolehmainen, & Rao, 2000; Nie, Liu, Zhan, & Guo, 2004).

3.2.3. Mass spectra

Mass spectrometry technique has been carried out to assist in the structural identification of the synthesized compounds. The mass spectra of the binary and ternary complexes, (**1**–**7**) are depicted in Fig. 7. The spectra of these complexes showed the highest mass peak with m/z at 373.00, 388.00, 586.00, 567.00, 436.00, 469.00 and 648.00 (calcd. 372.895, 390.270, 587.09, 569.30, 437.845,469.24 and 648.41 amu), which agree well with the suggested formula weights of the synthesized complexes, (**1**–**7**), respectively. Moreover, the peaks observed at m/z (%) = 222.00 (22.03), 219.00 (18.48), 220.00 (16.13), 221.00(22.82), 220.00 (1.63), 219.00 (7.76) and 219(7.40) give evidence about the presence of the organic ligand in these complexes, (**1**–**7**), respectively. In addition, the spectra exhibit peaks assignable to various fragments arising from the thermal cleavage of the complexes. The peak intensity gives an idea of the stability of the fragments. The most prominent mass spectral peaks are given in tabular form in Table 4 while Figs. 8–10 demonstrate the proposed paths of the decomposition steps for some metal complexes as representative example.

3.2.4. Electronic spectra and magnetic moment data

The geometry of the metal complexes has been deduced from their electronic spectra and magnetic measurements, Table 5. The effective magnetic moments for Ni^{2+} and Cu^{2+} complexes, (**1**) and (**2**,**5**) were 3.17, 2.01 and 1.98 B.M., respectively. The value of 3.17 B.M. for Ni^{2+} complex is typical for paramagnetic octahedral Ni^{2+}complexes with d^8 configuration and is close to the spin-only value (2.83 B.M.) (Mohamed & Abd El-Wahab, 2003; Skyrianou, Perdih, Turel, Kessissoglou, & Psomas, 2010). The value of 2.01 and 1.98 B.M. for the Cu^{2+} complexes was very close to the value for one unpaired electron and was in the range normally observed for the Cu^{2+} complexes (Abd El-Wahab & El-Sarrag, 2004; Para, 2004).

The solid reflectance spectrum of P-NaCMC shows maximum absorption band at 47619 cm^{-1} (210 nm) due to the carbonyl group (Bikova & Treimanis, 2004; Franco & Mercê, 2006). A comparison of the spectrum of P-NaCMC and its metal complexes showed the persistence of this band in all complexes that was slightly shifted to blue or red regions in the spectra of all metal complexes. Nickel (II) complex, (**1**) was found to be paramagnetic which excludes the possibility of square planar configuration. Its electronic spectrum show three electronic spectra bands in regions 12121, 18382 and 21978 cm^{-1} (825, 554 and 455 nm), respectively, suggesting octahedral configuration. The ground state for nickel (II) octahedral coordination is $^3A_{2g}$. Thus these transitions attributed to $^3A_{2g}$ (F) → $^3T_{2g}$ (F) (υ_1), $^3A_{2g}$ (F) → $^3T_{1g}$ (F) (υ_2) and $^3A_{2g}$ (F) → $^3T_{1g}$ (P) (υ_3) transition, respectively (Burkhardt, Görls, & Plass, 2008; Chavan & Sawant, 2010; Patel, Parekh, Panchal, & Patel, 2007). The electronic spectra of the Cu^{2+} complexes, (**2**,**5**) show two broad bands at 14,550–13,410 and 21,220–20,390 cm^{-1} (687–746 and 471–490 nm), respectively can be assigned to the electronic transitions $^2B_{1g} \rightarrow {}^2A_{1g}$ and $^2B_{1g} \rightarrow {}^2E_g$, respectively, which are relevant to distorted octahedral geometry around the central Cu^{2+} ion (Lakshmi, Reddy, & Raju, 2009; Shakir, Chishti, & Chingsubam, 2006). Ag^+ complexes, (**3**,**6**) are diamagnetic and have absorption bands at 24,390 and 25,641 cm^{-1} (410 and 390 nm), respectively and would be likely tetrahedral (Dinda & Sinha, 2003; Sakata, Yamaguchi, Shen, Hashimoto, & Tsuge, 2005). Also, UO_2(II) complexes, (**4**,**7**) are diamagnetic, their spectra showed new absorption bands at 20,833 and 21,739 cm^{-1} (480 and 460 nm), respectively which is attributed to the charge transfer transition, moreover they have coordination number eight and exists in dodecahedral geometry (Mashaly, Ramadan, El-Shetary, & Dawoud, 2005; Shebl, 2009; Shebl, Seleem, & El-Shetary, 2010).

3.2.5. Thermal analysis

In order to characterize the metal complexes more fully in terms of thermal stability, their thermal behaviors were studied. In the present investigation, the correlations between the different decomposition steps of P-NaCMC/complexes with the corresponding weight losses are discussed in terms of the proposed formula of P-NaCMC/complexes. The TGA curves are given in Figs. 11 and 12 and the data are listed in Table 6. The weight losses for each complex are calculated within the corresponding temperature ranges. Additionally, the obtained kinetic parameters data and Coats·Redfern plots for each step in the decomposition sequence of the metal complexes under study are summarized in Table 7 and represented in Fig. 13, respectively.

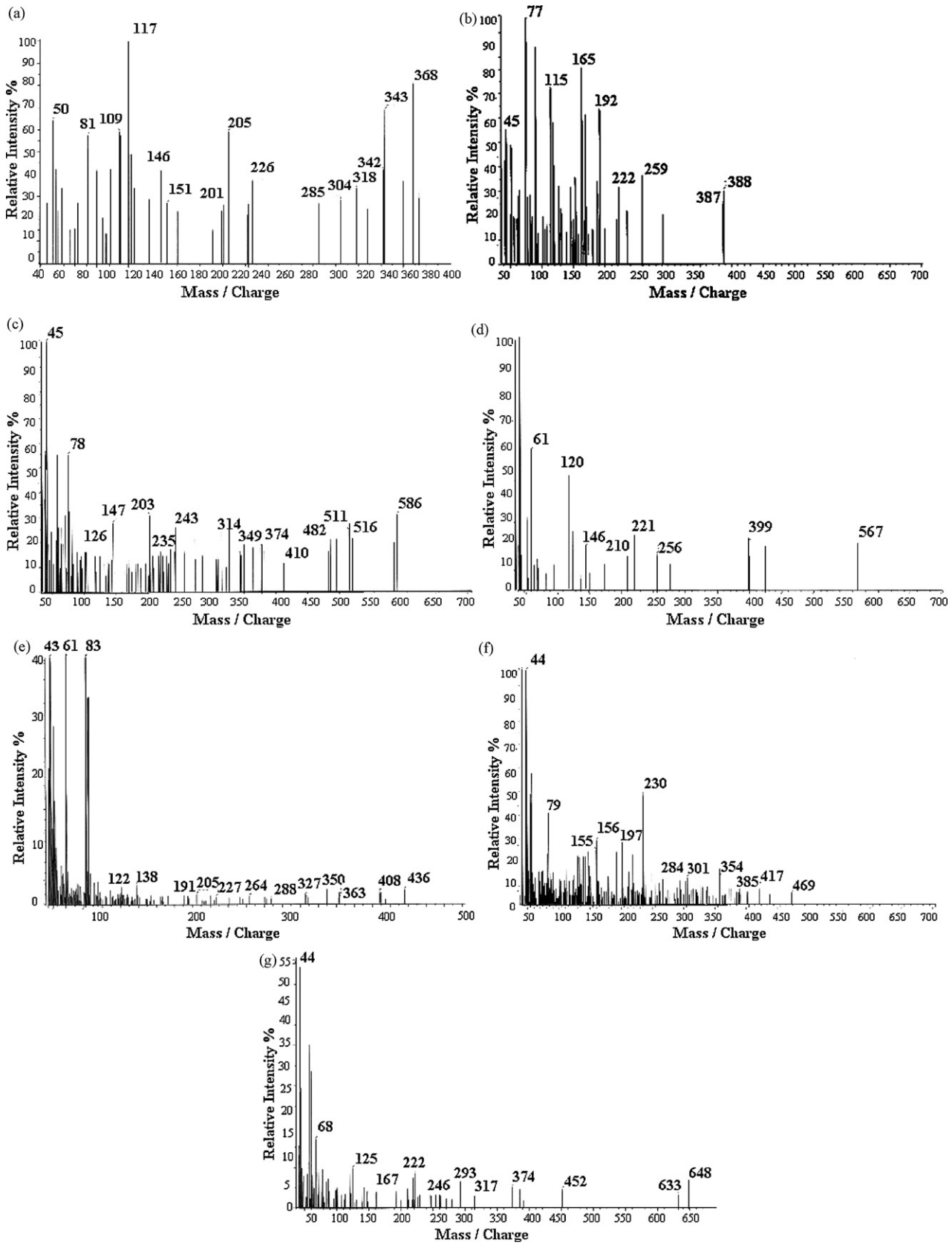

Fig. 7. Mass spectra of: (a) $[Ni(CMC)Cl(H_2O)_2]\cdot 1.25H_2O$, (b) $[Cu(CMC)(Cl)(H_2O)_2]\cdot 2H_2O$, (c) $[Ag_2(CMC_d)(H_2O)_4]\cdot 4.5H_2O$, (d) $[UO_2(CMC_d)(H_2O)_3]\cdot 1.5H_2O$, (e) $[Cu(CMC)(Py)Cl(H_2O)]\cdot 1.25H_2O$, (f) $[Ag(CMC)(Py)(H_2O)]\cdot 2.5H_2O$, (g) $[UO_2(CMC_d)(Py)(H_2O)_2]\cdot 2.5H_2O$.

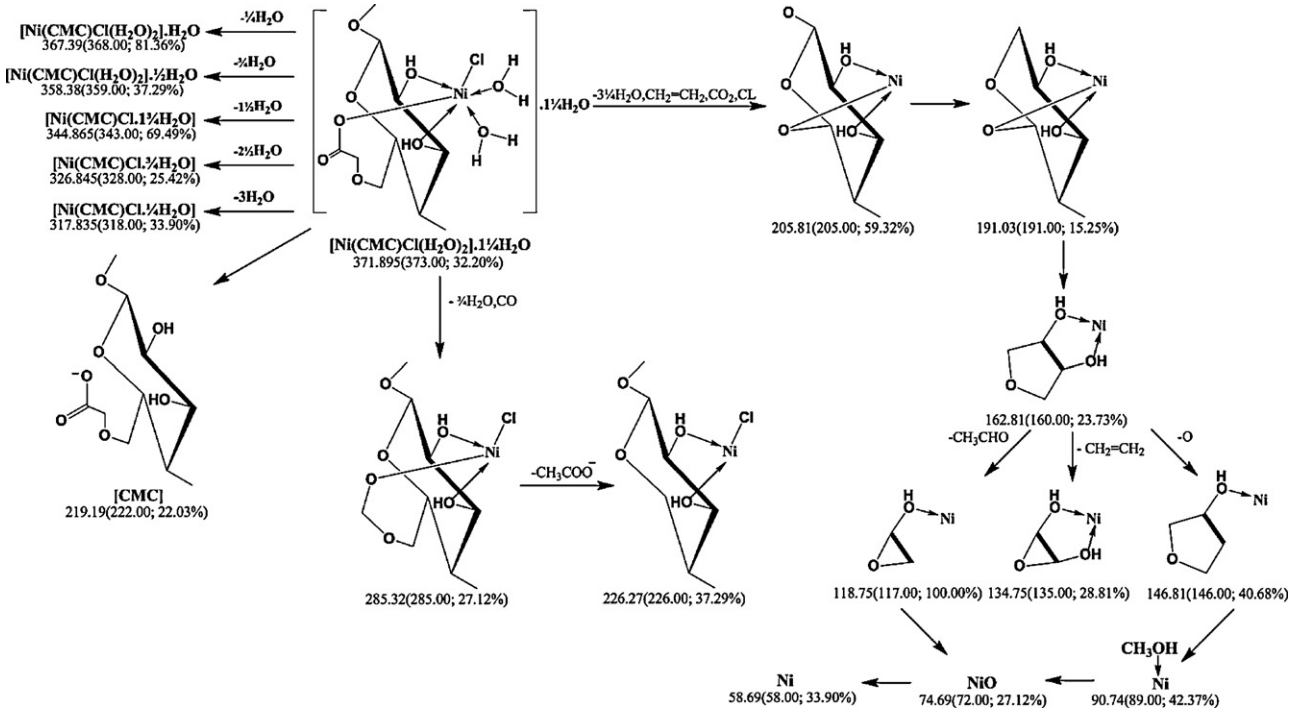

Fig. 8. Suggested fragmentation pathway of $[Ni(CMC)Cl(H_2O)_2]\cdot 1.25H_2O$; The values under each fragment denoted as calculated (found; intensity).

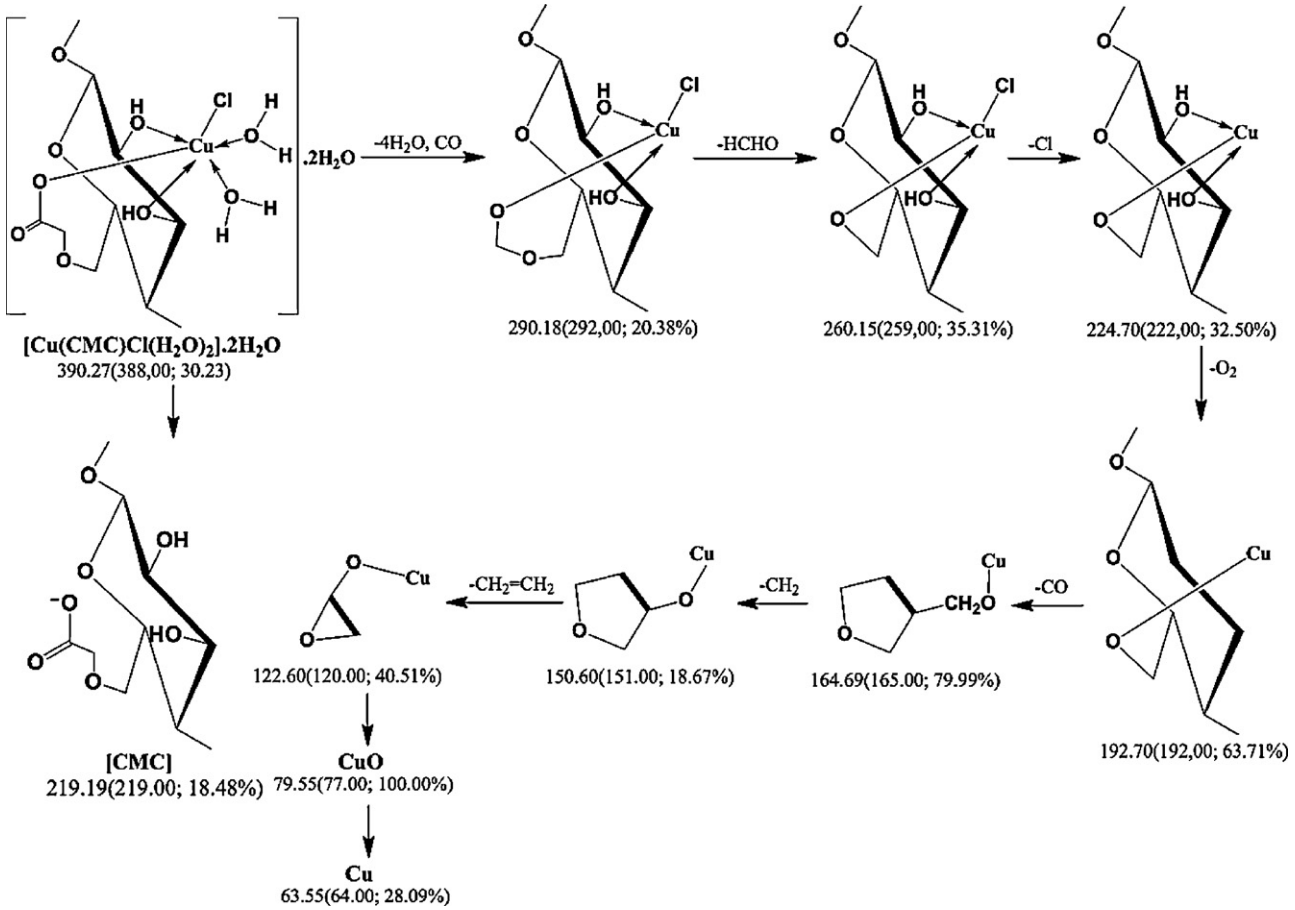

Fig. 9. Suggested fragmentation pathway of $[Cu(CMC)Cl(H_2O)_2]\cdot 2H_2O$; The values under each fragment denoted as calculated (found; intensity).

Table 4
The most relevant mass spectral peaks of binary and ternary complexes of P-NaCMC.

Compound no.	*m/z* Found (calcd.)	Relative intensity (%)	Loss moiety	Peak assignment due to loss moiety
(1) $NiC_8H_{11}O_7Cl{\cdot}3.25H_2O$	373.00(371.895)	32.20		
	285.00(285.32)	27.12	$3.25H_2O$ and CO	$NiC_7H_{11}O_6Cl$
	205.00(205.81)	59.32	CH_4, CO and Cl	$NiC_5H_7O_5$
	135.00(134.75)	28.81	CH≡CH, CO and OH	$NiC_2H_4O_3$
	117.00 (118.75)	100.00	O	$NiC_2H_4O_2$
	72.00 (74.69)	27.12	CH_4 and CO	NiO
	58.00 (58.69)	33.90	O	Ni
(2) $CuC_8H_{11}O_7Cl{\cdot}4H_2O$	388.00(390.27)	30.23		
	292.00(290.18)	20.38	$4H_2O$ and CO	$CuC_7H_{11}O_6Cl$
	259.00(260.15)	35.31	HCHO	$CuC_6H_9O_5Cl$
	222.00(224.70)	32.50	Cl	$CuC_6H_9O_5$
	192.00(192.70)	63.71	O_2	$CuC_6H_9O_3$
	165.00(164.69)	79.99	CO	$CuC_5H_9O_2$
	120.00(122.60)	40.51	$CH_3–CH{=}CH_2$	$CuC_2H_3O_2$
	77.00(79.55)	100.00	CH≡CH and OH	CuO
	64.00(63.55)	28.09	O	Cu
(3) $Ag_2C_8H_{10}O_7{\cdot}8.5H_2O$	586.00(587.09)	30.65		
	374.00(375.88)	17.74	$8.5H_2O$, O_2 and CH≡CH	$Ag_2C_6H_8O_5$
	349.00(346.86)	19.35	CHO	$Ag_2C_5H_7O_4$
	314.00(318.85)	22.58	CHO	$Ag_2C_4H_6O_3$
	274.00(275.75)	12.90	$CH_3–CH{=}CH_2$	Ag_2CO_3
	230.00(231.74)	12.90	CO_2	Ag_2O
	107.00(107.87)	16.13	O	2Ag
(4) $UO_2C_8H_{10}O_7{\cdot}4.5H_2O$	567.00(569.31)	17.95		
	399.00(400.14)	19.43	$4.5H_2O$, CO and CH_3COOH	$UO_2C_5H_6O_4$
	270.00(270.04)	7.07	CO_2,2CO and $CH_3–CH_3$	UO_2
(5) $CuC_{13}H_{16}NO_7Cl{\cdot}2.25H_2O$	436.00(437.85)	2.73		
	350.00(353.24)	2.25	$2.25H_2O$ and CH_3CHO	$CuC_{11}H_{12}NO_6Cl$
	327.00(325.23)	1.74	CO	$CuC_{10}H_{12}NO_5Cl$
	288.00(289.78)	1.06	Cl	$CuC_{10}H_{12}NO_5$
	191.00(192.68)	1.64	C_5H_4O-OH	$CuC_5H_7NO_3$
	97.00(97.57)	2.37	C_5H_5NO	$Cu(OH)_2$
	80.00(79.55)	2.44	H_2O	CuO
	61.00(63.55)	73.76	O	Cu
(6) $AgC_{13}H_{16}O_7N{\cdot}3.5H_2O$	469.00(469.24)	4.75		
	404.00(406.17)	6.23	$3.5H_2O$	$AgC_{13}H_{16}NO_7$
	326.00(327.06)	7.26	C_5H_5N	$AgC_8H_{11}O_7$
	299.00(299.05)	9.82	CO	$AgC_7H_{11}O_6$
	284.00(283.05)	11.74	O	$AgC_7H_{11}O_5$
	249.00(251.05)	17.08	O_2	$AgC_7H_{11}O_3$
	221.00(222.99)	5.98	$CH_2{=}CH_2$	$AgC_5H_7O_3$
	165.00(166.92)	3.29	$CH_2{=}CH_2$ and CO	CH_3COOAg
	123.00(122.91)	6.73	CO_2	CH_3Ag
	107.00(107.87)	15.08	CH_3	Ag
(7) $UO_2C_{13}H_{15}O_7N{\cdot}4.5H_2O$	648.00(648.41)	6.16		
	374.00(372.13)	5.16	$4.5H_2O$, C_5H_5N, $CH_2{=}CH_2$ and $2CO_2$	$UO_2C_4H_6O_3$
	270.00(270.03)	3.01	$CH_3–CH_3$, CO and CO_2	UO_2

Table 5
Magnetic moment and electronic spectral data of binary and ternary complexes.

Compound	Magnetic moment μ_{eff} (BM)	Absorption maxima (cm^{-1})	Assignment
(1)	3.17	12,121	$^3A_{2g}$ (F) → $^3T_{2g}$ (F)
		18,382	$^3A_{2g}$ (F) → $^3T_{1g}$ (F)
		21,978	$^3A_{2g}$ (F) → $^3T_{1g}$ (P)
(2)	2.01	14,550	$^2B_{1g} \rightarrow {}^2A_{1g}$
		21,220	$^2B_{1g} \rightarrow {}^2E_g$
(3)	Diamagnetic	24,390	–
(4)	Diamagnetic	20,833	–
(5)	1.98	13,410	$^2B_{1g} \rightarrow {}^2A_{1g}$
		20,390	$^2B_{1g} \rightarrow {}^2E_g$
(6)	Diamagnetic	25,641	–
(7)	Diamagnetic	21,739	–

1–4, binary complexes; 5–7, ternary complexes.

$[Ni(CMC)Cl(H_2O)_2]{\cdot}1.25H_2O$, (**1**) was thermally decomposed in five successive decomposition steps. The first decomposition step of estimated mass loss 6.06% (calculated mass loss 6.04%) is due to the elimination of one and quarter water molecule in the temperature ranges 50–100 °C. This dehydration range indicates the presence of hydrated water molecules in the complex. The second step occurs within the temperature range 100–213 °C with the estimated mass loss 4.62% (calculated mass loss 4.85%) may be attributed to the loss of one coordinated water molecule. The third step of decomposition occurs within the temperature range 213–260 °C with an estimated mass loss 14.38% (calculated mass loss 14.38%) which corresponds to the loss of another one coordinated water molecule and $0.5Cl_2$. The fourth step occurs within the temperature range 260–308 °C with the estimated mass loss 30.00% (calculated mass loss 29.47%) may be attributed to the pyrolysis of the organic ligand and loss of the organic moiety as 0.5CMC. The final step of the thermal decomposition in the temperature

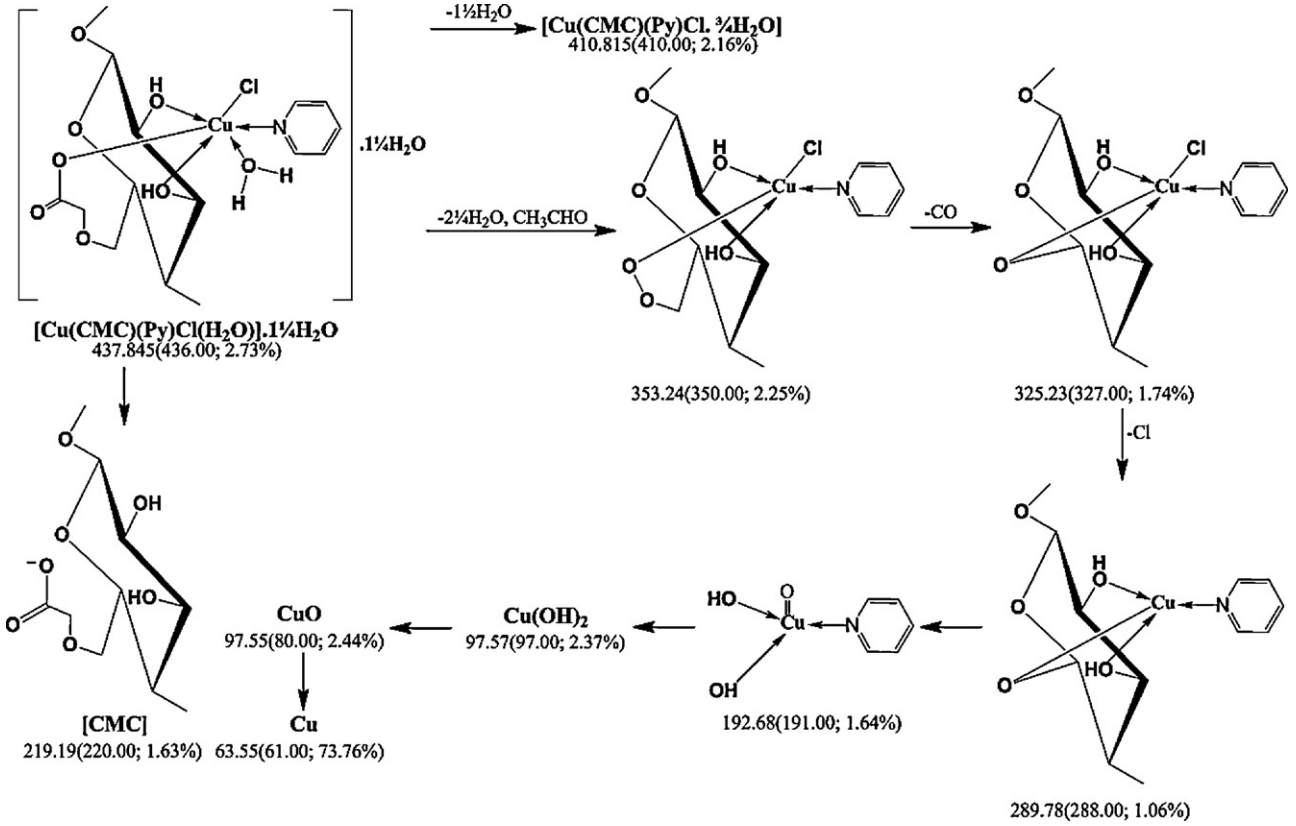

Fig. 10. Suggested fragmentation pathway of [Cu(CMC)(Py)Cl(H_2O)]·1.25 H_2O; The values under each fragment denoted as calculated (found; intensity).

range 308–452 °C with the estimated mass loss 29.01% (calculated mass loss 29.47%) is due to the complete decomposition of the organic ligand and loss of the remaining organic moiety as 0.5CMC. The remaining weight of 15.99% (calcd.15.78%) corresponds to the percentage of the Ni component indicating that the final decomposition product is Ni. The total estimated mass loss 84.01% (total calculated mass loss 84.23%).

[Cu(CMC)Cl(H_2O)$_2$].2H_2O, (**2**) was thermally decomposed in four successive decomposition stages. The first stage of decomposition occurring between 50 and 112 °C with the liberation of two hydrated water molecules with a corresponding estimated mass loss 9.30% (calculated mass loss 9.23%). The second step occurs within the temperature range 112–236 °C with the estimated mass loss 18.40% (calculated mass loss 18.32%) may be attributed to the loss of two coordinated water molecule and 0.5Cl_2. The third step of decomposition occurs within the temperature range 236–280 °C with an estimated mass loss 27.69% (calculated mass loss 28.08%) may be attributed to the pyrolysis of the organic ligand and loss of the organic moiety as 0.5CMC. The final step of the thermal

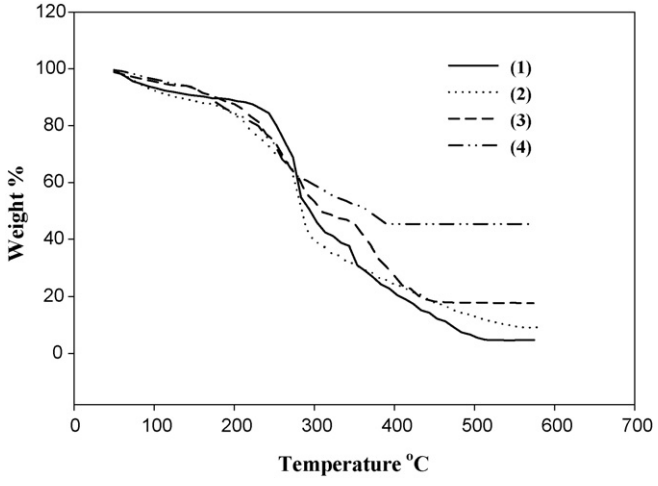

Fig. 11. TGA profile of binary complexes:
(**1**) [Ni(CMC)Cl(H_2O)$_2$]·1.25H_2O
(**2**) [Cu(CMC)(CMC)(H_2O)$_2$]·2H_2O
(**3**) [Ag_2(CMC_d)(H_2O)$_4$]·4.5H_2O
(**4**) [UO_2(CMC_d)(H_2O)$_3$]·1.5H_2O.

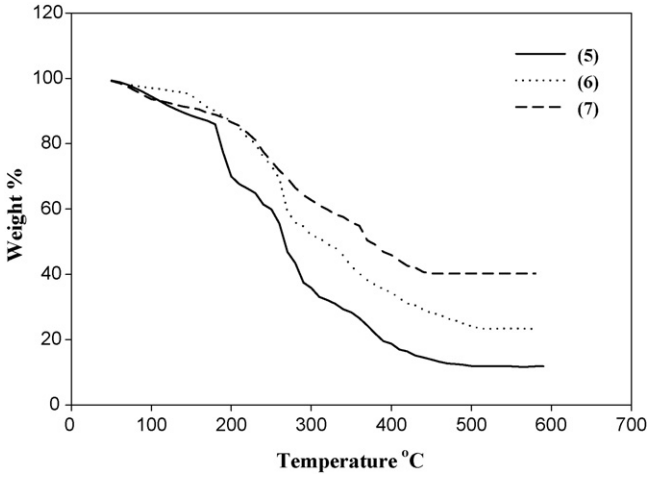

Fig. 12. TGA profile of ternary complexes:
(**5**) [Cu(CMC)(Py)Cl(H_2O)]·1.25H_2O
(**6**) [Ag(CMC)(Py)(H_2O)]·2·H_2O
(**7**) [UO_2(CMC_d)(Py)(H_2O)$_2$]·2.25H_2O.

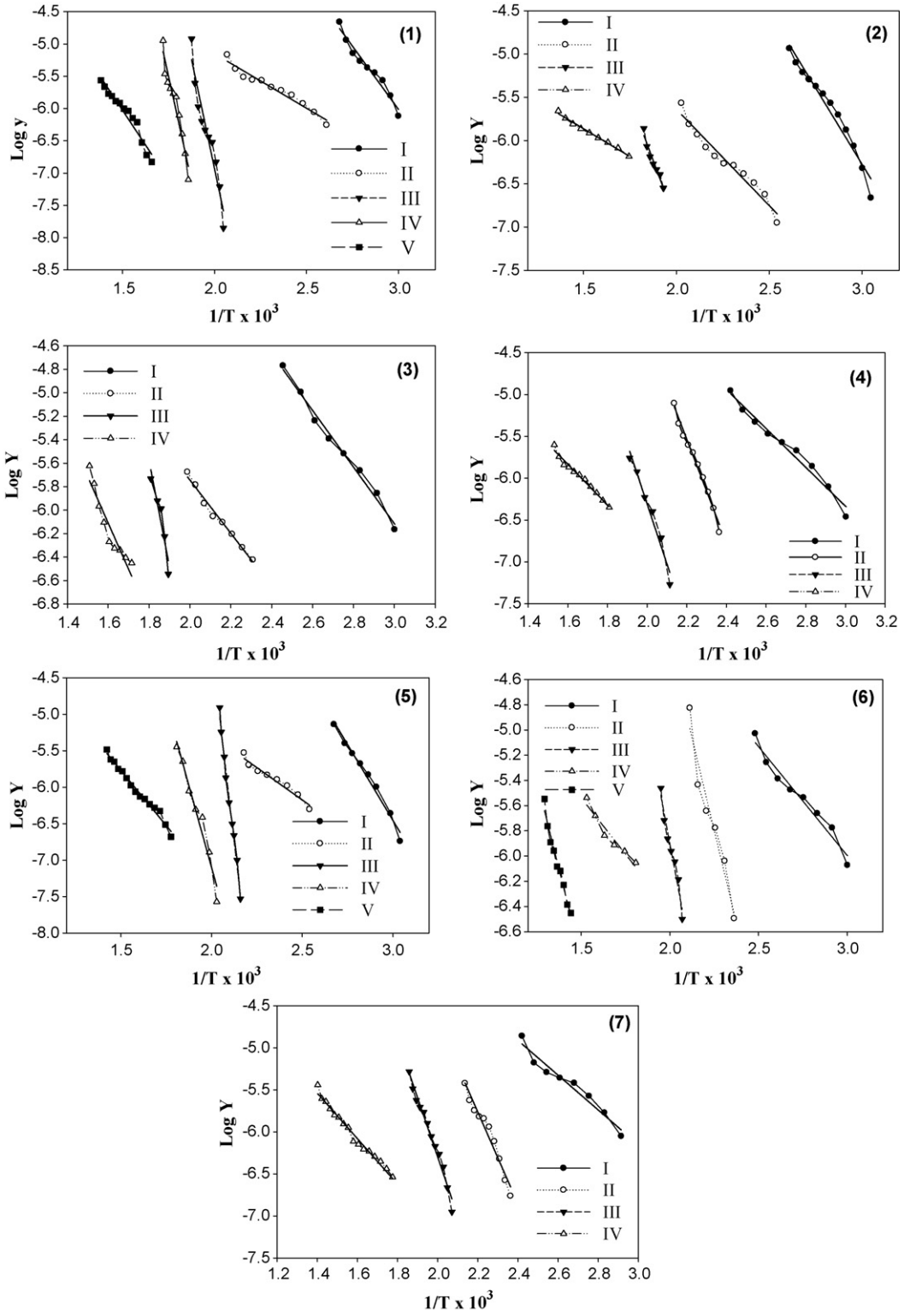

Fig. 13. Coats–Redfern plots of:
(**1**) $[Ni(CMC)Cl(H_2O)_2]\cdot 1.25H_2O$
(**2**) $[Cu(CMC)(Cl)(H_2O)_2]\cdot 2H_2O$
(**3**) $[Ag_2(CMC_d)(H_2O)_4]\cdot 4.5H_2O$
(**4**) $[UO_2(CMC_d)(H_2O)_3]\cdot 1.5H_2O$
(**5**) $[Cu(CMC)(Py)Cl(H_2O)]\cdot 1.25H_2O$
(**6**) $[Ag(CMC)(Py)(H_2O)]\cdot 2.5H_2O$
(**7**) $[UO_2(CMC_d)(Py)(H_2O)_2]\cdot 2.5H_2O$ $\log y = \log[\log\{W_f(W_f - W)^{-1}\}T^{-2}]$.

Table 6
Thermoanalytical and thermodynamic data of the thermal decomposition steps of binary and ternary complexes.

Compound no.	Stage	TG range (°C)	Mass loss	Total mass loss	Evolved moiety	Residue estimated (calc.) %
			Estimated (calc.)%			
(1) $[Ni(CMC)Cl(H_2O)_2]\cdot 1.25H_2O$	I	50–100	6.00(6.06)	84.01(84.23)	$1.25H_2O$ (hydr.)	$[Ni(CMC)Cl(H_2O)_2]$
	II	100–213	4.62(4.85)		$1H_2O$ (coord.)	$[Ni(CMC)Cl(H_2O)]$
	III	213–260	14.38(14.38)		$1H_2O$ (coord.) and $0.5Cl_2$	[Ni(CMC)]
	IV	260–308	30.00(29.47)		0.5CMC	[Ni(0.5CMC)]
	V	308–452	29.01(29.47)		0.5CMC	Ni; 15.99(15.78)
(2) $[Cu(CMC)Cl(H_2O)_2]\cdot 2H_2O$	I	50–112	9.30(9.23)	83.85(83.71)	$2H_2O$ (hydr.)	$[Cu(CMC)Cl(H_2O)_2]$
	II	112–236	18.40(18.32)		$2H_2O$(coord.) and $0.5Cl_2$	[Cu(CMC)]
	III	236–280	27.69(28.08)		0.5CMC	[Cu(0.5CMC)]
	IV	280–480	28.46(28.08)		0.5CMC	Cu; 16.15(16.28)
(3) $[Ag_2(CMC_d)(H_2O)_4]\cdot 4.5H_2O$	I	50–134	3.46(3.07)	62.90(63.43)	H_2O (hydr.)	$[Ag_2(CMC_d)(H_2O)_4]\cdot 3.5H_2O$
	II	134–244	22.30(23.02)		$3.5H_2O$ (hydr.) and $4H_2O$ (coord.)	$[Ag_2(CMC_d)]$
	III	244–288	18.23(18.67)		$0.5CMC_d$	$[Ag_2(0.5CMC_d)]$
	IV	288–396	18.91(18.67)		$0.5CMC_d$	2Ag; 37.10(36.75)
(4) $[UO_2(CMC_d)(H_2O)_3]\cdot 1.5H_2O$	I	50–141	5.69(4.75)	52.67(52.57)	$1.5H_2O$ (hydr.)	$[UO_2CMC_d(H_2O)_3]$
	II	141–196	8.66(9.50)		$3H_2O$ (coord.)	$[UO_2(CMC_d)]$
	III	196–260	19.03(19.16)		$0.5CMC_d$	$[UO_2(0.5CMC_d)]$
	IV	260–389	19.29(19.16)		$0.5CMC_d$	UO_2; 47.33(47.43)
(5) $[Cu(CMC)(Py)Cl(H_2O)]\cdot 1.25H_2O$	I	50–104	5.00(5.14)	84.90(85.48)	$1.25H_2O$ (hydr.)	$[Cu(CMC)(Py)Cl(H_2O)]$
	II	104–188	12.11(12.21)		$1H_2O$ (coord.) and $0.5Cl_2$	[Cu(CMC)(Py)]
	III	188–216	17.89(18.07)		Py	[Cu(CMC)]
	IV	216–284	25.00(25.03)		0.5CMC	[Cu(0.5CMC)]
	V	284–440	24.90(25.03)		0.5CMC	Cu; 15.10(14.51)
(6) $[Ag(CMC)(Py)(H_2O)]\cdot 2.5H_2O$	I	50–134	3.46(3.84)	76.48(77.01)	H_2O (hydr.)	$[Ag(CMC)(Py)(H_2O)_2]\cdot 0.5H_2O$
	II	134–200	10.14(9.60)		$1.5H_2O$ (hydr.) and $2H_2O$ (coord.)	[Ag(CMC)(Py)]
	III	200–244	16.40(16.86)		Py	[Ag(CMC)]
	IV	244–400	35.00(35.03)		0.75CMC	[Ag (0.25CMC)]
	V	400–503	11.48(11.68)		0.25CMC	Ag; 23.52(22.99)
(7)$\cdot[UO_2(CMC_d)(Py)(H_2O)_2]\cdot 2.5H_2O$	I	50–141	7.89(6.95)	58.21(58.36)	$2.5H_2O$ (hydr.)	$[UO_2(CMC_d)(Py)(H_2O)_2]$
	II	141–200	5.13(5.56)		$2H_2O$ (coord.)	$[UO_2(CMC_d)(Py)]$
	III	200–268	11.69(12.20)		Py	$[UO_2(CMC_d)]$
	IV	268–448	33.50(33.65)		CMC_d	UO_2; 41.79(41.65)

CMC, carboxymethyl cellulose; CMC_d, deprotonated form of carboxymethyl cellulose; Py, pyridine scondary ligand.

decomposition in the temperature range 280–480 °C with the estimated mass loss 28.46% (calculated mass loss 28.08%) is due to the complete decomposition of the organic ligand and loss of the remaining organic moiety as 0.5CMC. The remaining weight of 16.15% (calcd. 16.28%) corresponds to the percentage of the Cu component indicating that the final decomposition product is Cu. The total estimated mass loss 83.85% (total calculated mass loss 83.71%).

$[Ag_2(CMC_d)(H_2O)_4]\cdot 4.5H_2O$, (**3**) decomposed in four successive decomposition steps. The first decomposition step of estimated mass loss 3.46% (calculated mass loss 3.07%) is due to the elimination of one hydrated water molecule in the temperature ranges 50–134 °C. The second step occurs within the temperature range 134–244 °C with the estimated mass loss 22.30% (calculated mass loss 23.02%) may be attributed to the loss of three and half hydrated water molecule and four coordinated water molecule. The third step of decomposition occurs within the temperature range 244–288 °C with an estimated mass loss 18.23% (calculated mass loss 18.67%) may be attributed to the pyrolysis of the organic ligand and loss of the organic moiety as $0.5(CMC_d)$. The final step of the thermal decomposition in the temperature range 288–396 °C with the estimated mass loss 18.91% (calculated mass loss 18.67%) is due to the complete decomposition of the organic ligand and loss of the remaining organic moiety as $0.5(CMC_d)$. The remaining weight of 37.10% (calcd. 36.75%) corresponds to the percentage of the Ag component indicating that the final decomposition product is 2Ag. The total estimated mass loss 62.90% (total calculated mass loss 63.43%).

$[UO_2(CMC_d)(H_2O)_3]\cdot 1.5H_2O$, (**4**) was thermally decomposed in four successive decomposition steps. The first decomposition step takes place in the temperature ranges 50–141 °C. This step has weight losses of 5.69% (calculated mass loss 4.75%) showing the thermal liberation of one and half hydrated water molecule. The second step occurs within the temperature range 141–196 °C with the estimated mass loss 8.66% (calculated mass loss 9.50%) may be attributed to the loss of three coordinated water molecule. The third step of decomposition occurs within the temperature range 196–260 °C with an estimated mass loss 19.03% (calculated mass loss 19.16%) may be correlated with the pyrolysis of the organic ligand and loss of the organic moiety as 0.5(CMC). The final step of the thermal decomposition in the temperature range 260–389 °C with the estimated mass loss 19.29% (calculated mass loss 19.16%) is due to the complete decomposition of the organic ligand and loss of the remaining organic moiety as 0.5(CMC). The remaining weight of 47.33% (calcd. 47.43%) corresponds to the percentage of the UO_2 component indicating that the final decomposition product is UO_2. The total estimated mass loss 52.67% (total calculated mass loss 52.57%).

$[Cu(CMC)(Py)Cl(H_2O)]\cdot 1.25H_2O$, (**5**) was thermally decomposed in five successive decomposition steps. The first decomposition step of estimated mass loss 5.00% (calculated mass loss 5.14%) is due to the elimination of one and quarter hydrated water molecule in the temperature ranges 50–104 °C. The second step occurs within the temperature range 104–188 °C with the estimated mass loss 12.11% (calculated mass loss 12.21%) may be attributed to the loss of one coordinated water molecule and $0.5Cl_2$. The third step of

Table 7
Thermoanalytical and thermodynamic data of the thermal decomposition steps of binary and ternary complexes.

Sample	Stage	TG range (°C)	DTGA peak (°C)	A (s^{-1})	ΔS^* ($J\,K^{-1}\,mol^{-1}$)	ΔH^* ($kJ\,mol^{-1}$)	ΔG^* ($kJ\,mol^{-1}$)	E^* ($kJ\,mol^{-1}$)
(1) $[Ni(CMC)Cl(H_2O)_2]\cdot1.25H_2O$	I	50–100	71	1.41×10^{12}	−0.013	72.26	76.68	75.03
	II	100–213	124	18.77×10^{3}	−0.166	29.07	94.78	32.373
	III	213–260	228	2.13×10^{11}	−0.032	104.68	120.88	108.84
	IV	260–308	277	9.86×10^{10}	−0.040	105.15	126.91	109.73
	V	308–452	352	7547348	−0.119	77.23	151.88	82.43
(2) $[Cu(CMC)Cl(H_2O)_2]\cdot2H_2O$	I	50–112	69	4.55×10^{10}	−0.042	64.60	79,07	67.46
	II	112–236	210	94.36×10^{3}	−0.154	38.604	112.85	42.62
	III	236–280	278	1.66×10^{11}	−0.035	106.46	125.86	111.04
	IV	280–480	465	97.89	−0.214	18.51	176.73	24.65
(3) $[Ag_2(CMC_d)(H_2O)_4]\cdot4.5H_2O$	I	50–134	60	46.47×10^{4}	−0.118	39.13	78.49	41.89
	II	134–244	230	91.15×10^{3}	−0.154	39.22	116.86	43.41
	III	244–288	258	3.29×10^{17}	0.086	169.22	123.74	173.63
	IV	288–396	363	40.6×10^{5}	−0.125	70.20	149.52	75.48
(4) $[UO_2(CMC_d)(H_2O)_3]\cdot1.5H_2O$	I	50–141	65	64.92×10^{5}	−0.116	41.65	80.7	44.46
	II	141–196	163	2.16×10^{13}	0.007	103.67	100.53	107.30
	III	196–260	255	2.5×10^{12}	−0.012	111.19	117.69	115.58
	IV	260–389	375	17.96×10^{3}	−0.170	41.14	151.28	46.53
(5) $[Cu(CMC)(Py)Cl(H_2O)]\cdot1.25H_2O$	I	50–104	101	2.21×10^{10}	−0.049	76.48	94.73	79.59
	II	104–188	188	13.09×10^{2}	−0.189	30.11	117.19	33.94
	III	188–216	200	1.71×10^{10}	−0.053	80.41	105.41	84.34
	IV	216–284	261	1.03×10^{14}	0.018	167.68	157.82	172.12
	V	284–440	440	15.71×10^{2}	−0.191	51.91	188.11	57.84
(6) $[Ag(CMC)(Py)(H_2O)]\cdot2.5H_2O$	I	50–134	58	17.47×10^{4}	−0.146	30.35	78.50	33.11
	II	134–200	158	6.55×10^{11}	−0.022	91.25	100.63	94.83
	III	200–244	227	4.88×10^{11}	−0.026	101.56	114.29	105.72
	IV	244–400	263	15.92×10^{2}	−0.189	29.70	130.76	34.16
	V	400–503	404	1.66×10^{08}	−0.094	102.37	166.25	108.00
(7) $[UO_2(CMC_d)(Py)(H_2O)_2]\cdot2.5H_2O$	I	50–141	76	19.74×10^{6}	−0.107	44.40	81.60	47.31
	II	141–200	189	6.08×10^{12}	−0.004	100.57	102.34	104.41
	III	200–268	236	2.82×10^{14}	0.027	130.65	116.76	134.88
	IV	268–448	363	31.75×10^{3}	−0.165	46.57	151.57	51.87

DTG_{max}: maximum degradation temperature.

decomposition occurs within the temperature range 188–216 °C with an estimated mass loss 17.89% (calculated mass loss 18.07%) which corresponds to the loss of pyridine molecule. The fourth step occurs within the temperature range 216–284 °C with the estimated mass loss 25.00% (calculated mass loss 25.03%) may be attributed to the pyrolysis of the organic ligand and loss of the organic moiety as 0.5CMC. The final step of the thermal decomposition in the temperature range 284–440 °C with the estimated mass loss 24.90% (calculated mass loss 25.03%) is due to the complete decomposition of the organic ligand and loss of the remaining organic moiety as 0.5CMC. The remaining weight of 15.10% (calcd. 14.51%) corresponds to the percentage of the Cu component indicating that the final decomposition product is Cu. The total estimated mass loss 84.90% (total calculated mass loss 85.48%).

$[Ag(CMC)(Py)(H_2O)]\cdot2.5H_2O$, (**6**) was thermally decomposed in five successive decomposition steps. The first decomposition step of estimated mass loss 3.46% (calculated mass loss 3.84%) is due to the elimination of one hydrated water molecule in the temperature ranges 50-134 °C. The second step occurs within the temperature range 134–200 °C with the estimated mass loss 10.14% (calculated mass loss 9.60%) may be attributed to the loss of one and half hydrated water molecule and one coordinated water molecule. The third step of decomposition occurs within the temperature range 200–244 °C with an estimated mass loss 16.40% (calculated mass loss 16.86%) which corresponds to the loss of pyridine molecule. The fourth step occurs within the temperature range 244–400 °C with the estimated mass loss 35.00% (calculated mass loss 35.03%) may be attributed to the pyrolysis of the organic ligand and loss of the organic moiety as 0.75CMC. The final step of the thermal decomposition in the temperature range 400–503 °C with the estimated mass loss 11.48% (calculated mass loss 11.68%) is due to the complete decomposition of the organic ligand and loss of the remaining organic moiety as 0.25CMC. The remaining weight of 23.52% (calcd. 22.99%) corresponds to the percentage of the Ag component indicating that the final decomposition product is Ag. The total estimated mass loss 76.48% (total calculated mass loss 77.01%).

$[UO_2(CMC_d)(Py)(H_2O)_2]\cdot2.5H_2O$, (**7**) was thermally decomposed in four successive decomposition steps. The first decomposition step of estimated mass loss 7.89% (calculated mass loss 6.95%) is due to the elimination of two and half hydrated water molecule in the temperature ranges 50–141 °C. The second step occurs within the temperature range 141–200 °C with the estimated mass loss 5.13% (calculated mass loss 5.56%) may be attributed to the loss of two coordinated water molecule. The third step of decomposition occurs within the temperature range 200–268 °C with an estimated mass loss 16.40% (calculated mass loss 16.86%) which corresponds to the loss of pyridine molecule. The final step of the thermal decomposition in the temperature range 268–448 °C with the estimated mass loss 33.50% (calculated mass loss 33.65%) is due to the complete pyrolysis of the organic ligand and loss of the organic moiety as CMC_d. The remaining weight of 41.79% (calcd. 41.65%) corresponds to the percentage of the UO_2 component indicating that the final decomposition product is UO_2. The total estimated mass loss 58.21% (total calculated mass loss 58.36%).

3.2.5.1. The thermal decompositions mechanism and thermal stability of metal complexes. The solid metal complexes under study

are stable at the room temperature and decompose progressively during heating. The thermal decompositions of these complexes may be divided into two parts; dehydration followed by pyrolytic decomposition. The dehydration processes in which the removal of water molecules (hydrated followed by coordinated) of all complexes take place in two stages except Ni^{2+} binary complex, (**1**) which shows three stages. After removal of water molecules, the pyrolytic decomposition of a complex molecule starts to loss chloride anion followed by pyridine (in ternary complexes) and finally loss of carboxymethyl cellulose. It is clear that, the loss of carboxymethyl cellulose take place in two stages in all metal complexes except UO_2^{2+} ternary complex, (**7**) which losses carboxymethyl cellulose in one stage. All the complexes undergo thermal decomposition to form the corresponding metallic residue as the final products. The following equations indicate these results.

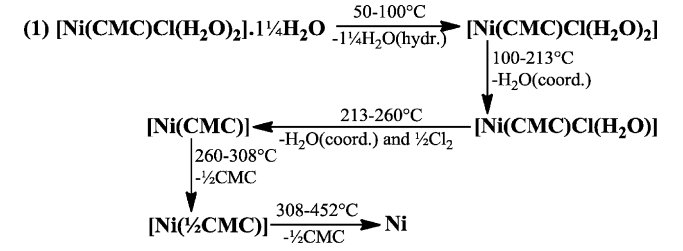

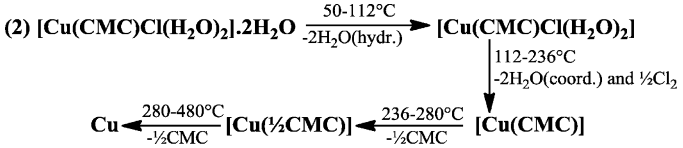

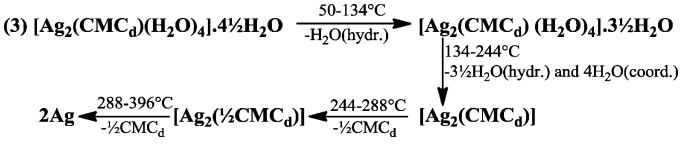

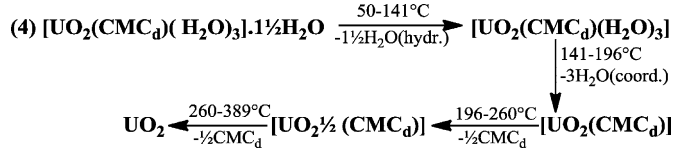

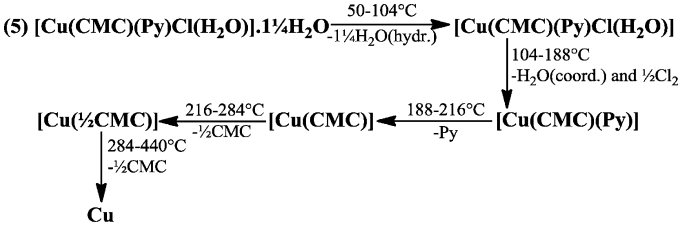

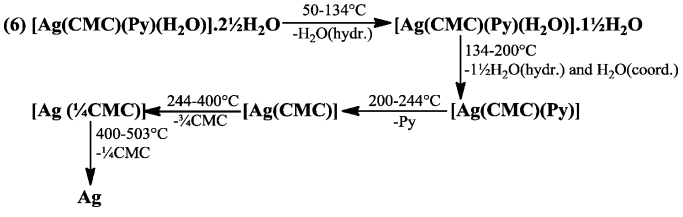

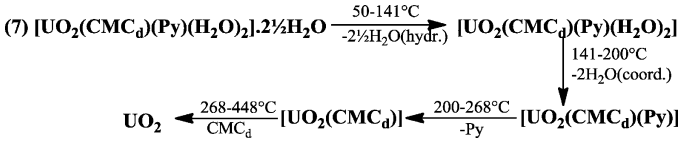

The relative stability of the complexes may be discussed in two ways: kinetic stability usually expressed as the activation energy values of decomposition reactions or thermal stability given as the temperature values at which decomposition begins (İçbudak, Yilmaz, & Ölmez, 1996).

Depending on the kinetic results, Table 7, the energies of activation for the first decomposition reaction were 75.03, 67.46, 41.89 and 44.46 kJ mol^{-1} for binary complexes, (**1**–**4**), respectively and it may be said that the thermal stability for these complexes follows the order: Ni^{2+}(**1**) > Cu^{2+}(**2**) > UO_2^{2+}(**4**) > Ag^{+}(**3**). Additionally, the sequence of the thermal stability of the ternary complexes follows the order: Cu^{2+}(**5**) > UO_2^{2+}(**7**) > Ag^{+}(**6**) where the activation energy values of these complexes are 79.59, 47.31 and 33.11 kJ mol^{-1}, respectively. Moreover, on the basis of the first DTG_{max} of the decompositions which taken as a parameter of thermal stability (Yeşilel & Ölmez, 2006; Yeşilel, Ölmez, and İçbudak, 2007), it is clear that: The thermal stability of the binary complexes follows the order: Ni^{2+} (71 °C) > Cu^{2+} (69 °C) > UO_2^{2+} (65 °C) > Ag^{+} (60 °C) and the sequence of the thermal stability of the ternary complexes follows the order: Cu^{2+} (101 °C) > UO_2^{2+} (76 °C) > Ag^{+} (58 °C).

On comparison of the thermal stability of all metal complexes, it is evident that:

The sequence of the thermal stability follows the order $Ni^{2+} > Cu^{2+} > UO_2^{2+} > Ag^{+}$ and this conform to that the thermal stabilities of the complexes increase as the ionic radii decreased (Basu, Shannigrahi, Ray, & Bagchi, 2005).

Ternary complexes are more stable than the binary complexes except one complex and this trend may be related to presence of pyridine moiety. The exception was the Ag^{+} ternary complex, (**6**) is less stable than Ag^{+} binary complex, (**3**) and this may be related to increasing of silver content in Ag^{+} binary complex, (**3**).

3.2.6. X-ray analysis

The X-ray diffractogram was used to investigate the crystal structure and assess the compatibility of P-NaCMC and its binary and ternary complexes in addition to study the influence of the metal ions on crystalline regions of the P-NaCMC. The X-ray diffractograms of the P-NaCMC and its binary and ternary complexes were recorded between 4° and 70° (2θ) and depicted in Fig. 14. It could be seen that there was a noticeable differences of peak height, width and position between the compounds under study. X-ray diffraction data of P-NaCMC and its binary and ternary complexes, Table 8 show that P-NaCMC gave a strong characteristic reflection at 2θ about 22.63 which corresponds to the interplanar distance d = 3.93 Å. Both the binary complexes, (**1**,**2**) and the ternary complexes, (**5**,**6**) still showed strong reflections but with different intensities at approximately the same value of 2θ in addition to other peaks appearing at different positions of 2θ value accompaind with shefiting in interplanar distance (d) contrasted to P-NaCMC pattern. This may be attributed to the rearrangement in the morphology of the polymeric chain of P-NaCMC as a result of complexation with metal ions. On comparison of these complexes, (**1**,**2**,**5**,**6**) it is evident that, their defractograms show similar features, indicating their isostructural nature and the effect of metal ions on crystallinity of uncomplexed P-NaCMC follows the order Ni^{2+}(**1**) = Ag^{+}(**6**) > Cu^{2+}(**5**) > Cu^{2+}(**2**). Additionally, in the diffraction spectra of silver binary complex, (**3**) and both uranyl complexes, (**4**,**7**), the peak at 2θ about 22.63 was even disappeared

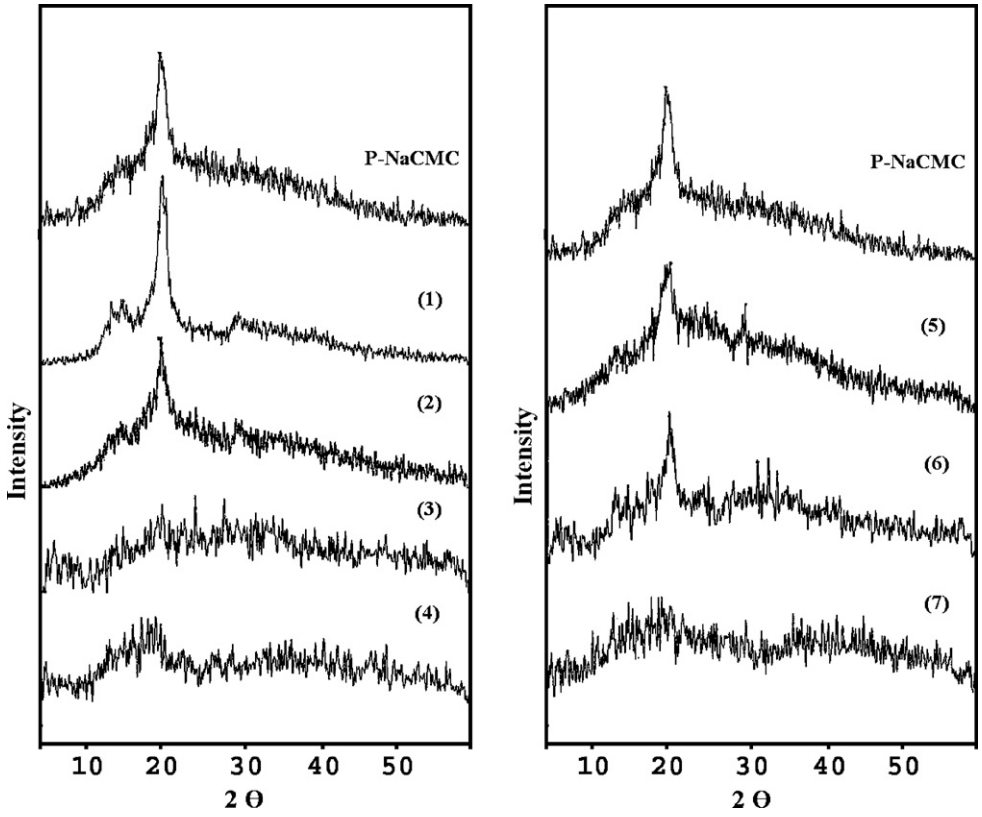

Fig. 14. X-ray diffraction patterns of P-NaCMC and both binary and ternary complexes:
(**1**) $[Ni(CMC)Cl(H_2O)_2]\cdot 1.25H_2O$
(**2**) $[Cu(CMC)(Cl)(H_2O)_2]\cdot 2H_2O$
(**3**) $[Ag_2(CMC_d)(H_2O)_4]\cdot 4.5H_2O$
(**4**) $[UO_2(CMC_d)(H_2O)_3]\cdot 1.5H_2O$
(**5**) $[Cu(CMC)(Py)Cl(H_2O)]\cdot 1.25H_2O$
(**6**) $[Ag(CMC)(Py)(H_2O)]\cdot 2.5H_2O$
(**7**) $[UO_2(CMC_d)(Py)(H_2O)_2]\cdot 2.5H_2O$.

accompanied with non appearance of other peaks and so, these metal complexes became amorphous. Moreover, it may be say that, the presence of pyridine moiety has an effect on the crystalline nature of P-NaCMC as clear from the comparison of crystallinity index value of copper complexes, (**5**, 0.72 > **2**, 0.69) as well as silver complexes, (**6**, 0.80 > **3,** . . .). Generally, X-ray diffraction spectra of complexed P-NaCMC show more numerous and sharper X-ray diffraction bands than uncomplexed P-NaCMC. This pattern consisted with the study of other similar complexes revealing the formation of a new crystalline phase (Wang, Du, & Liu, 2004).

On the basis of all above characterization, the tentative structures of the metal complexes are shown in Figs. 15 and 16.

Table 8
X-ray diffraction data of ligand, and its binary and ternary complexes.

Complex compound	2-θ (°)	d (Å)	I (%)	L (nm)[a]	Cr·I[a]
P-NaCMC	15.944	5.554	45.00	4.030	0.738
	22.632	3.926	100.00		
(1)	15.066	5.876	33.80	7.561	0.804
	16.755	5.287	34.50		
	22.700	3.914	100.00		
(2)	16.620	5.330	47.20	4.653	0.686
	22.767	3.903	100.00		
(3)	–	–	–	–	–
(4)	–	–	–	–	–
(5)	15.129	5.851	47.10	4.485	0.720
	23.302	3.814	100.00		
	30.191	2.958	66.70		
	34.784	2.577	72.50		
(6)	22.565	3.937	100.00	6.363	0.804
	36.144	2.483	69.30		
	37.833	2.376	72.40		
	39.184	2.297	61.10		
(7)	–	–	–	–	–

[b]CI, crystallinity index based on Segal's equation (Gümüskaya, Usta, & Kirci, 2003; He, Tang, & Wang, 2007; Jonoobi, Harun, Mathew, Hussein, & Oksman, 2010).
[a] L, size of crystallite based on Scherrer equation (He et al., 2007).

4. Antimicrobial assessments

The main aim of the production and synthesis of any antimicrobial compound is to inhibit the causal microbe without any side effects on the patients. In addition, it is worthy to stress here on the basic idea of applying any chemotherapeutic agent which depends essentially on the specific control of only one biological function and not multiple ones. The chemotherapeutic agent affecting only one function has a highly sounding application in the field of treatment by anticancer, since most anticancers used in the present time affect both cancerous diseased cells and healthy ones which in turns affect the general health of the patients. Therefore, there is a real need for having a chemotherapeutic agent which controls only one function (El-Sharief, Ammar, Ammar, & Zaki, 1983).

In testing the antimicrobial activity of our compounds more than one test organism was used to increase the chance of detecting antibiotic principles in tested materials. The antimicrobial activities were done against standard strains of Gram-positive bacteria *S. aureus* (ATCC 25923), *S. pyogenes* (ATCC 19615), Gram-negative bacteria *P. phaseolicola* (GSPB 2828), *P. fluorescens* (S

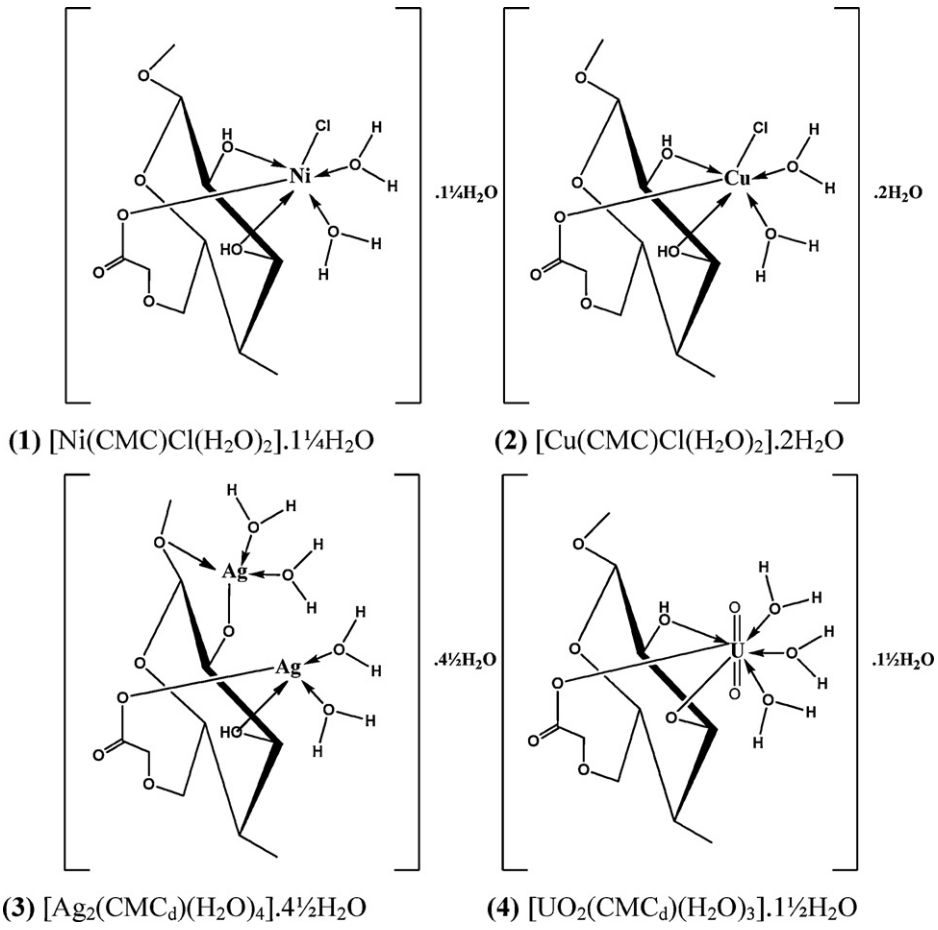

Fig. 15. Suggested structure of the binary complexes of P-NaCMC
(**1**) $[Ni(CMC)Cl(H_2O)_2]\cdot 1.25H_2O$ (2) $[Cu(CMC)Cl(H_2O)_2]\cdot 2H_2O$ (**3**) $[Ag_2(CMC_d)(H_2O)_4]\cdot 4.5H_2O$ (4) $[UO_2(CMC_d)(H_2O)_3]\cdot 1.5H_2O$.

97) as well as fungi *F. oxysporum* and *A. fumigates* at concentration of 1 and 2 mg/ml using the agar disc diffusion method (Uruş et al., 2005). The screening data obtained for the compounds under study; P-NaCMC, binary and ternary complexes, metal salts and control against the sensitive organisms expressed as the diameter of growth inhibition area in mm are summarized in Table 9 and depicted in Figs. 17 and 18. Additionally, the activity index (%) was calculated (Abd El–Wahab, 2008b; Singh et al., 2008) and summarized in Table 10 and represented in Figs. 19 and 20.

Table 9
Antimicrobial screening results of all compounds under study.

Sample	Gram-positive bacteria				Gram-negative bacteria				Fungi			
	Staphylococcus aureus (ATCC 25923)		*Streptococcus pyogenes* (ATCC 19615)		*Pseudomonas phaseolicola* (GSPB 2828)		*Pseudomonas fluorescens* (S 97)		*Fusarium oxysporum*		*Aspergillus fumigatus*	
Concentration	2 mg/ml	1 mg/ml	2 mg/ml	1 mg/ml	2 mg/ml	1 mg/ml	2 mg/ml	1 mg/ml	2 mg/ml	1 mg/ml	2 mg/ml	1 mg/ml
P-NaCMC	3	–	–	–	–	–	–	–	–	–	–	–
(1)	3	–	3	–	13	6	–	–	–	–	4	–
(2)	6	5	4	3	10	5	5	–	31	28	3	–
(3)	5	4	3	–	6	4	16	11	–	–	5	3
(4)	3	–	–	–	6	3	5	3	20	16	–	–
(5)	12	9	9	6	14	7	–	–	32	26	8	4
(6)	6	3	–	–	8	5	17	11	–	–	4	–
(7)	3	–	–	–	10	5	–	–	–	–	5	–
$NiCL_2\cdot 6H_2O$	10	5	7	5	8	5	10	6	12	8	8	5
$CuCL_2\cdot 2H_2O$	14	9	10	7	5	3	8	4	14	10	8	6
$AgNO_3$	6	4	–	–	–	–	21	16	38	33	35	28
$UO_2(NO_3)_2\cdot 6H_2O$	23	18	22	16	3	–	9	5	16	10	14	8
Control	42	28	38	30	36	25	38	30	40	28	40	31

- The test was done using the agar disc diffusion method.
- Control: *Chloramphencol*, *Cephalothin* and *Cycloheximide* were used as control for Gram-positive bacteria, Gram-negative bacteria and antifungal, respectively.
- Inhibition values: (-) No effect; 3–12, low activity; 13–21, intermediate activity; 22–30, high activity and >30, very high activity.
- P-NaCMC, prepared sodium carboxymethyl cellulose.
- 1–4, binary complexes; 5–7, ternary complexes.

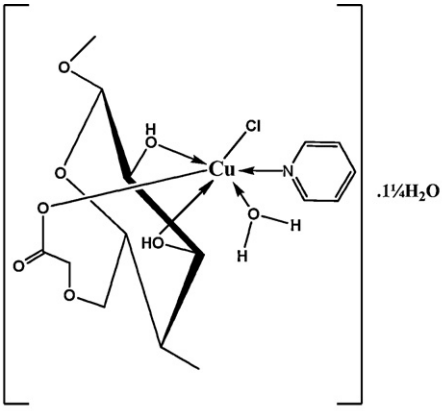

(5) $[Cu(CMC)(Py)Cl(H_2O)].1¼H_2O$

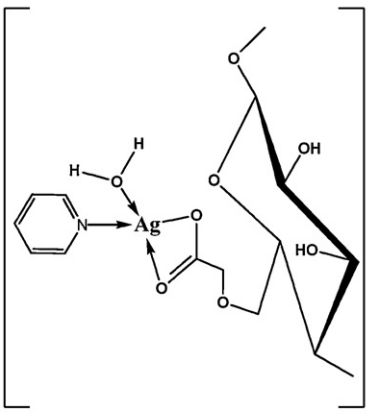

(6) $[Ag(CMC)(Py)(H_2O)].2½H_2O$

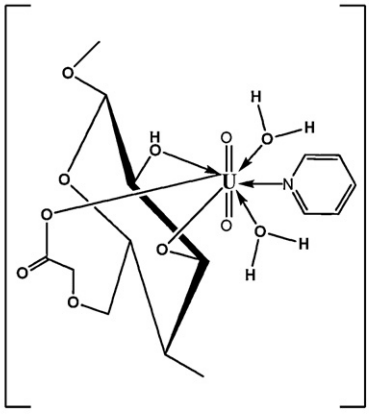

(7) $[UO_2(CMC_d)(Py)(H_2O)_2].2½H_2O$

Fig. 16. Suggested structure of the ternary complexes of P-NaCMC
(**5**) $[Cu(CMC)(Py)Cl(H_2O)]\cdot 1.25H_2O$
(**6**) $[Ag(CMC)(Py)(H_2O)]\cdot 2.5H_2O$ (7) $[UO_2(CMC_d)(Py)(H_2O)_2]\cdot 2.5H_2O$.

A comparison of all tested compounds towards the different organisms brings out the following facts to light:

- The compounds inhibit the growth of organisms to a greater extent as the concentration is increased (Abd El–Wahab, 2008b).
- P-NaCMC revealed to be totally inefficient against Gram-negative bacteria and fungi. It displays low activity against *S. aureus* only.
- The highest antimicrobial activity among the group of the tested compounds was observed against the *P. phaseolicola*, *P. fluorescens* and *F. oxysporum* and the most effective towards fungi strain; *F. oxysporum.*
- The biological activity of the P-NaCMC exhibited a considerable enhancement on coordination with the metal ions against all the test organisms under identical experimental conditions. This enhancement in activity suggests that the chelation could facilitate the ability of a complex to cross a cell membrane and can be explained on the basis of chelation theory (Abd El-Wahab & Faheim, 2009; Angelusiu et al., 2009). Chelation considerably

Table 10
Antimicrobial activity (% activity index) at higher concentration of all compounds under study.

	% Activity index										
	P-NaCMC	(1)	(2)	(3)	(4)	(5)	(6)	(7)	$NiCL_2.6H_2O$	$CuCL_2.2H_2O$	$AgNO_3$	$UO_2(NO_3)_2.6H_2O$
Gram-positive bacteria												
Staphylococcus aureus (*ATCC 25923*)	7.14	7.14	14.29	11.90	7.14	28.57	14.29	7.14	23.81	33.33	14.29	54.76
Streptococcus pyogenes (*ATCC 19615*)	–	7.89	10.53	7.89	–	23.68	–	–	18.42	26.32	–	57.98
Gram-negative bacteria												
Pseudomonas phaseolicola (GSPB 2828)	–	36.11	27.78	16.67	16.67	38.89	22.22	27.78	22.22	13.89	–	8.33
Pseudomonas fluorescens (S 97)	–	–	13.16	42.11	13.16	–	44.74	–	26.32	21.05	55.26	23.68
Fungi												
Fusarium oxysporum	–	–	77.50	–	50.00	80.00	–	–	30.00	35.00	95.00	40.00
Aspergillus fumigatus	–	10.00	7.50	12.50	–	20.00	10.00	12.50	20.00	20.00	87.50	35.00

- P-NaCMC; Prepared sodium carboxymethyl cellulose.
- 1–4, binary complexes.
- 5–7, ternary complexes.
- % Activity Index $= \frac{\text{Zone of inhibition by test compound (diameter)}}{\text{Zone of inhibition by standard (diameter)}} \times 100$.

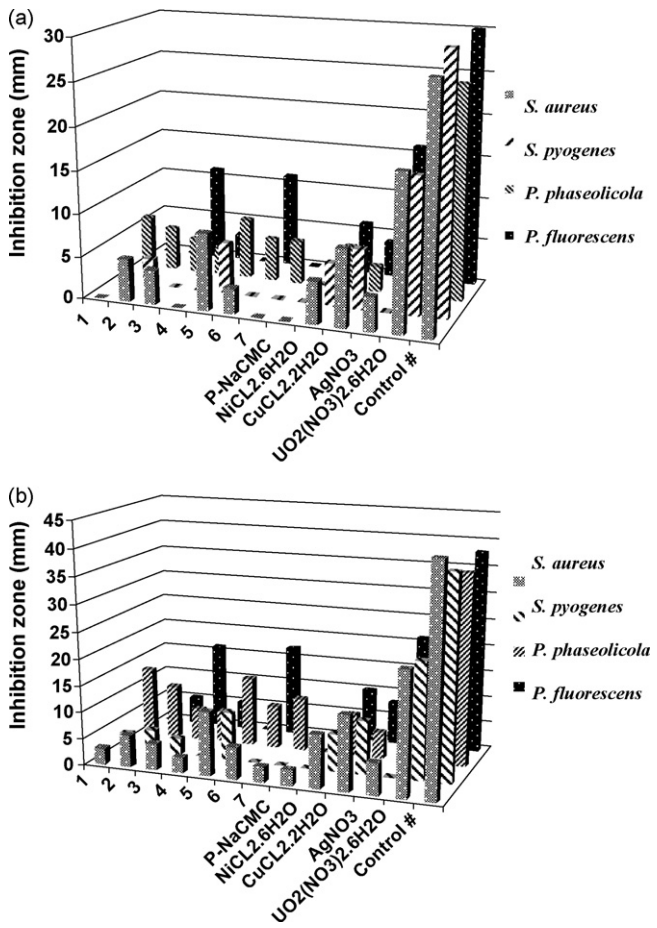

Fig. 17. Antibacterial activity of all compounds under study
(a) at low concentration 1 mg/ml (b) at high concentration 2 mg/ml.

reduces the polarity of the metal ion mainly because of partial sharing of its positive charge with the donor group and possible electron delocalization over the whole chelate ring. Such chelation could also enhance the lipophilic character of the central metal atom, which subsequently favours its permeation through the lipid layer of the cell membrane resulting in interference with normal cell processes.

- All metal complexes, (**1**–**7**) exhibited broader spectrum of activity against Gram-positive, Gram-negative bacteria and fungi. They have higher or equal activity against all organisms than the P-NaCMC.
- Cu^{2+} complexes; (**2**,**5**) were more active against one or more organism especially against *F. oxysporum*, they display very high activity comparable to the standard drug. These significant activities may arise from the presence of chloride anion. Additionally, $UO_2{}^{2+}$ complex, (**4**) has intermediate activity against *F. oxysporum*. The biological activity of the complexes are found to follow the order **5** > **2** > **4** > P-NaCMC and all remaining complexes. The importance of this lies in the fact that these complexes could be applied fairly in the treatment of some common diseases caused by *F. oxysporum.*
- All metal complexes, (**1**–**7**) display variable activity against the *P. phaseolicola*. Ni^{2+} and Cu^{2+} complexes (**1**,**5**) were the most potent antibacterial agent against *P. phaseolicola* confirming the suggestion that the chloride anion plays an important role in the antibacterial activity. They have intermediate activity. The biological activity of the complexes are found to follow the order **5** > 1 > **2** = **7** > **6** > **3** = **4** > P-NaCMC.
- Ag^{+} complexes, (**3**,**6**) display intermediate activity against *P. fluorescens,* while the other complexes have low activity and P-NaCMC did not register any activity.

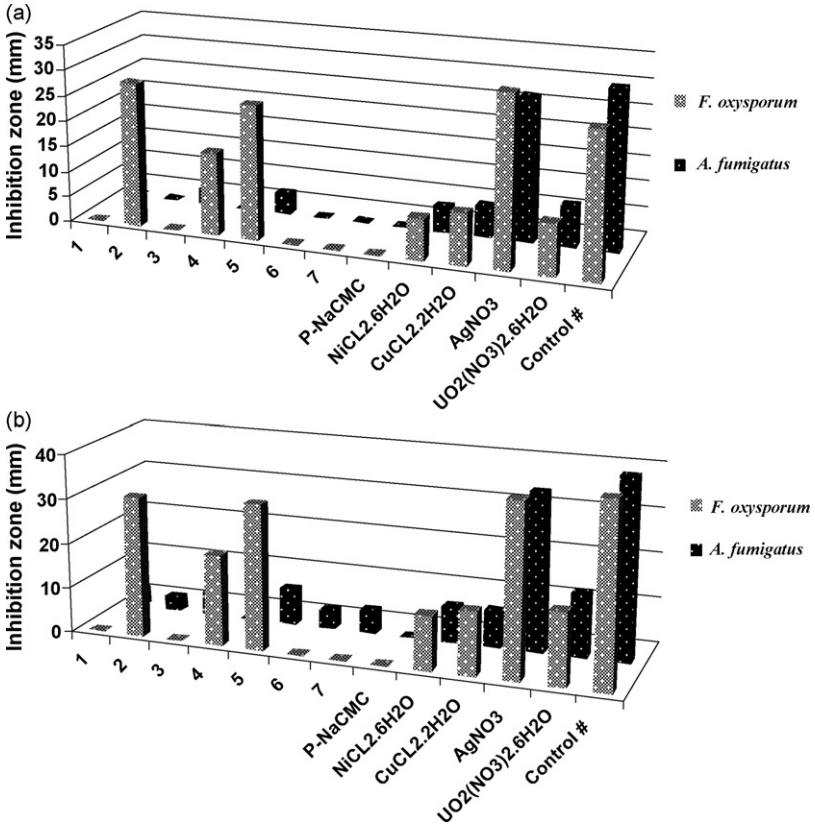

Fig. 18. Antifungi activity of all compounds under study. (a) at low concentration 1 mg/ml; (b) at high concentration 2 mg/ml.

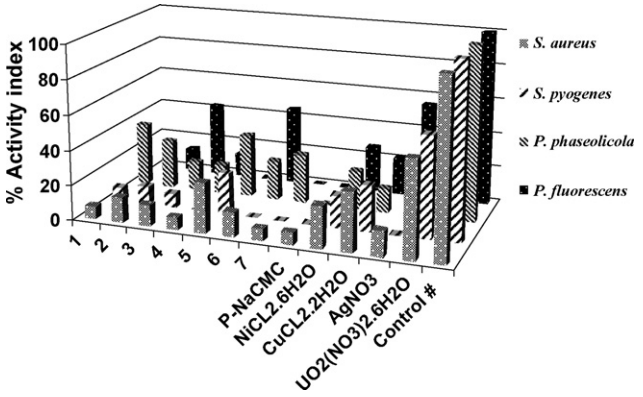

Fig. 19. Antibacterial activity (% activity index) at higher concentration of all compounds under study.

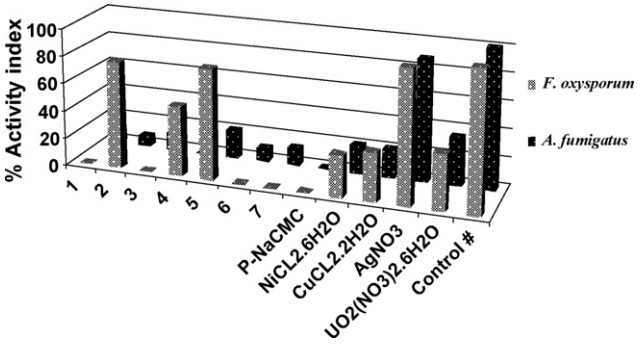

Fig. 20. Antifungi activity (% activity index) at higher concentration of all compounds under study.

- The % Activity Index data indicate the highest activity (28.57, 23.68, 38.89, 80.00 and 20.00%) for $[Cu(CMC)(Py)Cl(H_2O)]\cdot 1.25H_2O$, (**5**) against both the *S. aureus*, *S. pyogenes*, *P. phaseolicola*, *F. oxysporum* and *A. fumigatus* at the concentration of 2.0 mg/ml among all metal complexes.

5. Conclusion

The design and synthesis of binary and ternary complexes of Ni^{2+}, Cu^{2+}, Ag^{+} and $UO_2{}^{2+}$ with carboxymethyl cellulose in its sodium salt (P-NaCMC) and pyridine (py) in aqueous media have been successfully demonstrated. This work was undertaken to shed more light on the complexation behavior of cellulose in the presence of another ligand pyridine, in solid state, to help in understanding the mode of complexation of each ligand towards the metal ions. The coordination mode of P-NaCMC to be the two vicinal uncarboxylated diol groups (2- and 3-hydroxyl groups) of the glucopyranose rings in addition to the carbonyl oxygen atom of the carboxylate group while the coordination mode of pyridine ligand is the ring nitrogen. Generally, ternary complexes are more stable than the binary complexes and this trend may be related to presence of pyridine moiety. Moreover, it may be said that, the presence of pyridine moiety has an effect on the crystalline nature of P-NaCMC. Incorporating of metal ions enhances the antimicrobial properties of P-NaCMC against all the test organisms under identical experimental conditions and the screening data obtained suggest that these complexes belong to broad spectrum antimicrobial agents.

References

Abd El-Wahab, Z. H., & Faheim, A. A. (2009). Metal complexes of phosphorus compounds including indigoid structure: synthesis, characterization, and biological study. *Phosphorus, Sulfur, and Silicon*, *184*, 341–361.

Abd El–Wahab, Z. H., Mashaly, M. M., & Faheim, A. A. (2005). Synthesis and characterization of cobalt(II), cerium(III), and dioxouranium(VI) complexes of 2,3-dimethyl-1-phenyl 4-salicylidene-3-pyrazolin-5-one mixed ligand complexes, pyrolytic products, and biological activities. *Chemical Papers*, *59*(1), 25–36.

Abd El–Wahab, Z. H., Mashaly, M. M., Salman, A. A., & Faheim, A. A. (2004). Co(II), Ce(III) and UO_2(VI) bis-salicylatothiosemicarbazide complexes: Binary and ternary complexes, thermal studies and antimicrobial activity. *Spectrochimica Acta Part A*, *60*, 2861–2873.

Abd El-Wahab, Z. H., & El-Sarrag, M. R. (2004). Derivatives of phosphate Schiff base transition metal complexes: synthesis, studies and biological activity. *Spectrochimica Acta Part A: Molecular and Biomolecular Spectroscopy*, *60*, 271–277.

Abd El–Wahab, Z. H. (2008a). Complexation of 4-amino-1,3 dimethyl-2,6 pyrimidine dione derivatives with cobalt(II) and nickel(II) ions: Synthesis, spectral, thermal and antimicrobial studies. *Journal of Coordination Chemistry*, *61*(11), 1696–1709.

Abd El–Wahab, Z. H. (2008b). Mixed ligand complexes of nickel(II) and cerium(III) ions with 4-(-3-methoxy-4-hydroxyl benzylideneamino)-1,3dimethyl-2,6pyrimidine-dione and some nitrogen/oxygen donor ligands. *Journal of Coordination Chemistry*, *61*(20), 3284–3296.

Abd El–Wahab, Z. H. (2007). Mononuclear metal complexes of organic carboxylic acid derivatives: Synthesis, spectroscopic characterization, thermal investigation and antimicrobial activity. *Spectrochimica Acta Part A*, *67*, 25–38.

Abu El-Reash, G., El-Ayaan, U., Gabr, I. M., & El-Rachawy, E.-B. (2010). Transition metal complexes of Vanillin-4N-(2-pyridyl) thiosemicarbazone (H2VPT); thermal, structural and spectroscopic studies. *Journal of Molecular Structure*, *969*, 33–39.

Adel, A. M., Abd El–Wahab, Z. H., Ibrahim, A. A., & Al–Shemy, M. T. (2010). Characterization of microcrystalline cellulose prepared from lignocellulosic materials. Part I. Acid catalyzed hydrolysis. *Bioresource Technology*, *101*, 4446–4455.

Adinugraha, M. P., Marseno, D. W., & Haryadi. (2005). Synthesis and characterization of sodium carboxymethylcellulose from cavendish banana pseudo stem (*Musa cavendishii* LAMBERT). *Carbohydrate Polymers*, *62*, 164–169.

Angelusiu, M. V., Almajan, G. L., Rosu, T., Negoiu, M., Almajan, E.-R., & Roy, J. (2009). Copper(II) and uranyl(II) complexes with acylthiosemicarbazide: Synthesis, characterization, antibacterial activity and effects on the growth of promyelocytic leukemia cells HL-60. *European Journal of Medicinal Chemistry*, *44*, 3323–3329.

Barba, C., Montané, D., Rinaudo, M., & Farriol, X. (2002). Synthesis and characterization of carboxymethylcelluloses (CMC) from non-wood fibers I. Accessibility of cellulose fibers and CMC synthesis. *Cellulose*, *9*, 319–326.

Barba, C., Montané, D., Farriol, X., Desbrières, J., & Rinaudo, M. (2002). Synthesis and characterization of carboxymethylcelluloses from non-wood pulps II. Rheological behavior of CMC in aqueous solution. *Cellulose*, *9*, 327–335.

Bassett, J., Denney, R. C., Jeffery, G. H., & Mendham, J. (1978). *Vogel's textbook of quantitative inorganic analysis* (4th ed.). London: Longmans.

Basu, J. K., Shannigrahi, M., Ray, N., & Bagchi, S. (2005). UV–vis spectroscopic study of interaction of metal ions with the ET(30) dye involving micellar media. *Spectrochimica Acta Part A*, *61*, 2539–2542.

Bikova, T., & Treimanis, A. (2004). UV-absorbance of oxidized xylan and monocarboxyl cellulose in alkaline solutions. *Carbohydrate Polymers*, *55*, 315–322.

Biswal, D. R., & Singh, R. P. (2004). Characterisation of carboxymethyl cellulose and polyacrylamide graft copolymer. *Carbohydrate Polymers*, *57*, 379–387.

Bono, A., Ying, P. H., Yan, F. Y., Muei, C. L., Sarbatly, R., & Krishnaiah, D. (2009). Synthesis and characterization of carboxymethyl cellulose from palm kernel cake. *Advances in Natural and Applied Sciences*, *3*(1), 5–11.

Bontea, D., Mita, C., & Humelnicu, D. (2006). Removal of uranyl ions from wastewaters using cellulose and modified cellulose materials. *Journal of Radioanalytical and Nuclear Chemistry*, *268*(2), 305–311.

Burkhardt, A., Görls, H., & Plass, W. (2008). Nickel(II) complexes with Schiff-base ligands derived from epimeric pyranose backbones as 2,3-chelators: modeling the coordination chemistry of chitosan. *Carbohydrate Research*, *343*, 1266–1277.

Capitani, D., Porro, F., & Segre, A. L. (2000). High field NMR analysis of the degree of substitution in carboxymethyl cellulose sodium salt. *Carbohydrate Polymers*, *42*, 283–286.

Chavan, S. S., & Sawant, V. A. (2010). Synthesis, structural characterization, thermal and electrochemical studies of Mn(II), Co(II), Ni(II) and Cu(II) complexes containing thiazolylazo ligands. *Journal of Molecular Structure*, *965*, 1–6.

Chen, S., Zou, Y., Yan, Z., Shen, W., Shi, S., Zhang, X., et al. (2009). Carboxymethylated-bacterial cellulose for copper and lead ion removal. *Journal of Hazardous Materials*, *161*, 1355–1359.

Çolak, A. T., Yeşilel, O. Z., & Büyükgüngör, O. (2010). One-dimensional coordination polymer of zinc(II)-pyridine-2,5-dicarboxylate with N,N-dimethylethylenediamine: Synthesis, structural, spectroscopic and thermal properties. *Journal of Inorganic and Organometallic Polymers*, *20*, 26–31.

Dahou, W., Ghemati, D., Oudia, A., & Aliouche, D. (2010). Preparation and biological characterization of cellulose graft copolymers. *Biochemical Engineering Journal*, *48*, 187–194.

Dinda, J., & Sinha, C. (2003). Naphthyl-(2-pyridylmethylene)amine complexes of silver(I) and ruthenium(II): synthesis, spectral studies and electrochemical behavior. *Transition Metal Chemistry*, *28*, 864–870.

Du, B., Li, J., Zhang, H., Huang, L., Chen, P., & Zhou, J. (2009). Influence of molecular weight and degree of substitution of carboxymethylcellulose on the stability of acidified milk drinks. *Food Hydrocolloids*, *23*, 1420–1426.

Ejikeme, P. M. (2008). Investigation of the physicochemical properties of microcrystalline cellulose from agricultural wastes I: Orange mesocarp. *Cellulose*, *15*, 141–147.

El-Dissouky, A., El-Bindary, A. A., El-Sonbati, A. Z., & Hilali, A. S. (2001). Structural and models of dioxouranium(VI) with rhodanine azodyes—V. *Spectrochimica Acta Part A*, *57*, 1163–1170.

El-Sakhawy, M., & Hassan, M. L. (2007). Physical and mechanical properties of microcrystalline cellulose prepared from agricultural residues. *Carbohydrate Polymers*, *67*, 1–10.

El-Sharief, A. M. S., Ammar, M. S., Ammar, Y. A., & Zaki, M. E. A. (1983). 2,5-Dichlorobenzenesulphonamide derivatives & their biological activities. *Indian Journal of Chemistry (B)*, *22*, 700–704.

Fan, X., Liu, Z.-T., & Liu, Z.-W. (2010). Preparation and application of cellulose triacetate microspheres. *Journal of Hazardous Materials*, *177*, 452–457.

Ferrari, E., Grandi, R., Lazzari, S., & Saladini, M. (2005). Hg(II)-coordination by sugar-acids: Role of the hydroxy groups. *Journal of Inorganic Biochemistry*, *99*, 2381–2386.

Filipiuk, D., Fuks, L., & Majdan, M. (2005). Transition metal complexes with uronic acids. *Journal of Molecular Structure*, 744–747 705–709.

Franco, A. P., & Mercê, A. L. R. (2006). Complexes of carboxymethylcellulose in water. 1: Cu^{2+}, VO^{2+} and Mo^{6+}. *Reactive and Functional Polymers*, *66*, 667–681.

Franco, A. P., Recio, M. A. L., Szpoganicz, B., Delgado, A. L., Felcman, J., & Mercê, A. L. R. (2007). Complexes of carboxymethylcellulose in water. Part 2. Co^{2+} and Al^{3+} remediation studies of wastewaters with Co^{2+}, Al^{3+}, Cu^{2+}, VO^{2+} and Mo^{6+}. *Hydrometallurgy*, *87*, 178–189.

Fuks, L., Filipiuk, D., & Majdan, M. (2006). Transition metal complexes with alginate biosorbent. *Journal of Molecular Structure*, *792-793*, 104–109.

Groenewold, G. S., Jong, W. A., Oomens, J., & Stipdonk, M. J. V. (2010). Variable denticity in carboxylate binding to the uranyl coordination complexes. *Journal of American Society of Mass Spectrometry*, *21*, 719–727.

Gümüskaya, E., Usta, M., & Kirci, H. (2003). The effects of various pulping conditions on crystalline structure of cellulose in cotton linters. *Polymer Degradation and Stability*, *81*, 559–564.

Gurgel, L. V. A., Júnior, O. K., Gil, R. P. F., & Gil, L. F. (2008). Adsorption of Cu(II), Cd(II), and Pb(II) from aqueous single metal solutions by cellulose and mercerized cellulose chemically modified with succinic anhydride. *Bioresource Technology*, *99*, 3077–3083.

He, J., Tang, Y., & Wang, S.-Y. (2007). Differences in morphological characteristics of bamboo fibres and other natural cellulose fibres: Studies on X-ray diffraction, solid state 13C-CP/MAS NMR, and second derivative FTIR spectroscopy data. *Iranian Polymer Journal*, *16*(12), 807–818.

Hedlund, A., & Germgård, U. (2007). Some aspects on the kinetics of etherification in the preparation of CMC. *Cellulose*, *14*, 161–169.

İçbudak, H., Yilmaz, V. T., & Ölmez, H. (1996). Thermal decomposition behaviour of some trivalent transition and inner-transition metal complexes of triethanolamine. *Thermochimica Acta*, *289*, 23–32.

Jiang, L. Y., Li, Y., Zhang, L., & Wang, X. (2009). Preparation and characterization of a novel composite containing carboxymethyl cellulose used for bone repair. *Materials Science and Engineering C*, *29*, 193–198.

Jonoobi, M., Harun, J., Mathew, A. P., Hussein, M. Z. B., & Oksman, K. (2010). Preparation of cellulose nanofibers with hydrophobic surface characteristics. *Cellulose*, *17*, 299–307.

Junicke, H., Arendt, Y., & Steinborn, D. (2000). Synthesis and characterization of novel platinum(IV) complexes with functionalized carbohydrates. *Inorganic Chimica Acta*, *304*, 224–229.

Kutsenko, L. I., Bochek, A. M., Vlasova, E. N., & Volchek, B. Z. (2005). Synthesis of carboxymethyl cellulose based on short fibers and lignified part of flax pedicels (boon). *Russian Journal of Applied Chemistry*, *78*(12), 2014–2018.

Lakshmi, A. P. V., Reddy, P. S., & Raju, V. J. (2009). Synthesis, characterization and antimicrobial activity of 3d transition metal complexes of a biambidentate ligand containing quinoxaline moiety. *Spectrochimica Acta Part A: Molecular and Biomolecular Spectroscopy*, *74*, 52–57.

Li, M.-Y., Hu, P.-Z., Xu, K.-X., & Cai, L.-H. (2005). Synthesis and characterization of transition metal complexes of multidentate ligands containing a pyridine ring; synthesis and reactivity in inorganic. *Metal-Organic and Nano-Metal Chemistry*, *35*, 333–338.

Li, W., Sun, B., & Wu, P. (2009). Study on hydrogen bonds of carboxymethyl cellulose sodium film with two-dimensional correlation infrared spectroscopy. *Carbohydrate Polymers*, *78*, 454–461.

Lii, C.-Y., Tomasik, P., Zaleska, H., Liaw, S.-C., & Lai, V. M-F. (2002). Carboxymethyl cellulose-gelatin complexes. *Carbohydrate Polymers*, *50*, 19–26.

Ma, J., Xu, Y., Fan, B., & Liang, B. (2007). Preparation and characterization of sodium carboxymethylcellulose/poly(N-isopropylacrylamide)/clay semi-IPN nanocomposite hydrogels. *European Polymer Journal*, *43*, 2221–2228.

Mashaly, M. M., Abd El–Wahab, Z. H., & Faheim, A. A. (2004a). Mixed-ligand complexes of a Schiff base, 8-hydroxyquinoline and oxalic acid with Cu(II), Ni(III), Zn(II), and Fe(III) ions: Pyrolytic products and biological activities. *Synthesis and Reactivity in Inorganic and Metal-Organic Chemistry*, *34*(2), 233–268.

Mashaly, M. M., Abd El–Wahab, Z. H., & Faheim, A. A. (2004b). Preparation, spectral characterization and antimicrobial activities of Schiff base complexes derived from 4-aminoantipyrine. Mixed ligand complexes with 2-aminopyridine, 8 hydroxyquinoline and oxalic acid and their pyrolytical products. *Journal of Chinese Chemical Society*, *51*, 901–915.

Mashaly, M. M., Ramadan, A. T., El-Shetary, B. A., & Dawoud, A. K. (2005). Synthesis and characterization of new transition and actinide metal complexes of a hydrazone ligand. Mixed-ligand complexes, pyrolysis products, and biological activity. synthesis and reactivity in inorganic. *Metal-Organic, and Nano-Metal Chemistry*, *34*, 1319–1348.

Melander, M., & Vourinen, T. (2001). Determination of the degree of polymerisation of carboxymethyl cellulose by size exclusion chromatography. *Carbohydrate Polymers*, *46*, 227–233.

Mohamed, G. G., & Abd El-Wahab, Z. H. (2003). Salisaldehyde-2-aminobenzimidazole schiff base complexes of Fe(III), Co(II), Ni(II), Cu(II), Zn(II) and Cd(II). *Journal of Thermal Analysis and Calorimetry*, *73*, 347–359.

Mohamed, G. G., & Abd El –Wahab, Z. H. (2005). Mixed ligand complexes of bis(phenylimine) Schiff base ligands incorporating pyridinium moiety: Synthesis, characterization and antibacterial activity. *Spectrochimica Acta Part A*, *61*, 1059–1068.

Mostafa, M. M., & Aicha, Y.-N. (2002). Dioxouranium(VI) complexes of some macrocyclic ligands derived from 2,6-diformyl- and 2,6-diacetylpyridines and some aliphatic and aromatic amines. *Synthesis and Reactivity in Inorganic Metal-Organic Chemistry*, *32*(1), 143–154.

Mukhopadhyay, A, Kolehmainen, E., & Rao, C. P. (2000). Lanthanide-saccharide chemistry: synthesis and characterisation of Ce(III)-saccharide complexes. *Carbohydrate Research*, *324*, 30–37.

Naves, A. F., & Petri, F. S. D. (2005). The effect of molecular weight and degree of substitution on the interactions between carboxymethyl cellulose and cetyltrimethylammonium bromide. *Colloids and Surfaces A: Physicochemistry in Engineering Aspects*, *254*, 207–214.

Nie, H., Liu, M., Zhan, F., & Guo, M. (2004). Factors on the preparation of carboxymethylcellulose hydrogel and its degradation behavior in soil. *Carbohydrate Polymers*, *58*, 185–189.

Nishat, N., Ahmad, S., Rahisuddin, & Ahamad, T. (2006). Synthesis and characterization of antibacterial polychelates of urea–formaldehyde resin with Cr(III), Mn(II), Fe(III), Co(II), Ni(II), Cu(II), and Zn(II) metal ions. *Journal of Applied Polymer Science*, *100*, 928–936.

Norkus, E., Vaičiūnienė, J., Vuorinen, T., & Macalady, D. L. (2004). Equilibria of Cu(II) in alkaline suspensions of cellulose pulp. *Carbohydrate Polymers*, *55*, 47–55.

Ohwoavworhua, F. O., & Adelakun, T. A. (2005). Some physical characteristics of microcrystalline cellulose obtained from raw cotton of *Cochlospermum planchonii*. *Tropical Journal of Pharmaceutical Research*, *4*(2), 501–507.

Oudhoff, K. A., Buijtenhuij, F. A. , (Ab), Wijnen, P. H., Schoenmakers, P. J., & Kok, W. Th. (2004). Determination of the degree of substitution and its distribution of carboxymethylcelluloses by capillary zone electrophoresis. *Carbohydrate Research*, *339*, 1917–1924.

Papageorgiou, S. K., Kouvelos, E. P., Favvas, E. P., Sapalidis, A. A., Romanos, G. E., & Katsaros, F. K. (2010). Metal–carboxylate interactions in metal–alginate complexes studied with FTIR spectroscopy. *Carbohydrate Research*, *345*, 469–473.

Para, A. (2004). Complexation of metal ions with dioxime of dialdehyde starch. *Carbohydrate Polymers*, *57*, 277–283.

Patel, S. H., Parekh, H. M., Panchal, P. K., & Patel, M. N. (2007). Polymeric coordination compounds derived from transition metal(II) with tetradentate Schiff-base: Synthetic, spectroscopic, magnetic and thermal approach. *Journal of Macromolecular Science. Part A*, *44*, 599–603.

Peydecastaing, J., Vaca-Garcia, C., & Borredon, E. (2009). Accurate determination of the degree of substitution of long chain cellulose esters. *Cellulose*, *16*, 289–297.

Pushpamalar, V., Langford, S. J., Ahmad, M., & Lim, Y. Y. (2006). Optimization of reaction conditions for preparing carboxymethyl cellulose from sago waste. *Carbohydrate Polymers*, *64*, 312–318.

Ren, J.-L., Sun, R.-C., & Peng, F. (2008). Carboxymethylation of hemicelluloses isolated from sugarcane bagasse. *Polymer Degradation and Stability*, *93*, 786–793.

Rodríguez, A., Moral, A., Serrano, L., Labidi, J., & Jiménez, L. (2008). Rice straw pulp obtained by using various methods. *Bioresource Technology*, *99*, 2881–2886.

Ruzene, D. S., Goncalves, A. R., Teixeira, J. A., & Pessoa De Amorim, M. T. (2007). Carboxymethylcellulose obtained by ethanol/water organosolv process under acid conditions. *Applied biochemistry and biotechnology*, *136/140*, 573–582.

Sacarescu, L., Ardeleanu, R., Sacarescu, G., Simionescu, M., & Mangalagiu, I. (2007). Polysilane–metal complexes for organic semiconductors. *High Performance Polymers*, *19*, 501–509.

Sakata, K., Yamaguchi, Y., Shen, X., Hashimoto, M., & Tsuge, A. (2005). Synthesis and spectroscopic properties of cobalt(II), copper(I), and silver(I) complexes and crystal structure of a cobalt(II) complex with a bidentate diisonitrile containing two amino nitrogens in the bridging group. *Synthesis and Reactivity in Inorganic, Metal-Organic, and Nano-Metal Chemistry*, *35*, 545–551.

Shakir, M., Chishti, H.-T.-N., & Chingsubam, P. (2006). Metal ion-directed synthesis of 16-membered tetraazamacrocyclic complexes and their physico-chemical studies. *Spectrochimica Acta Part A: Molecular and Biomolecular Spectroscopy*, *64*, 512–517.

Shebl, M., Seleem, H. S., & El-Shetary, B. A. (2010). Ligational behavior of thiosemicarbazone, semicarbazone and thiocarbohydrazone ligands towards VO(IV), Ce(III), Th(IV) and UO_2(VI) ions: Synthesis, structural characterization and biological studies. *Spectrochimica Acta Part A: Molecular and Biomolecular Spectroscopy*, *75*, 428–436.

Shebl, M. (2009). Synthesis, spectral and magnetic studies of mono- and bi-nuclear metal complexes of a new bis(tridentate NO_2) Schiff base ligand derived from 4,6-diacetylresorcinol and ethanolamine. *Spectrochimica Acta Part A: Molecular and Biomolecular Spectroscopy*, *73*, 313–323.

Shoukry, A. A., & Shoukry, M. M. (2008). Coordination properties of hydralazine Schiff base Synthesis and equilibrium studies of some metal ion complexes. *Spectrochimica Acta Part A*, *70*, 686–691.

Singh, V. P., Singh, A., & Singh, S. (2008). Synthesis, structural studies, and antimicrobial activity of polymeric copper(II) tetrathiocyanato diargentate(I) complexes with some acylhydrazones. *Journal of Applied Polymer Science*, *110*, 1336–1343.

Skyrianou, K. C., Perdih, F., Turel, I., Kessissoglou, D. P., & Psomas, G. (2010). Nickel-quinolones interaction. Part 2: Interaction of nickel(II) with the antibacterial drug oxolinic acid. *Journal of Inorganic Biochemistry*, *104*, 161–170.

Stigsson, V., Kloow, G., Germgård, U., & Andersson, N. (2005). The influence of cobalt (II) in carboxymethyl cellulose processing. *Cellulose*, *12*, 395–401.

Suflet, D. M., Chitanu, G. C., Valentin, I., & Popa, V. I. (2006). Phosphorylation of polysaccharides: New results on synthesis and characterisation of phosphorylated cellulose. *Reactive & Functional Polymers*, *66*, 1240–1249.

Sundar, S. T., Sain, M. M., & Oksman, K. (2010). Characterization of microcrystalline cellulose and cellulose long fiber modified by iron salt. *Carbohydrate Polymers*, *80*, 35–43.

Szorcsik, A., Nagy, L., Scopelliti, M., Pellerito, L., & Sipos, P. (2006). Characterization of complexes formed between $[Me_2Sn(IV)]^{2+}$ and carboxymethylcelluloses. *Carbohydrate Research*, *341*, 2083–2089.

Toğrul, H., & Arslan, N. (2003). Production of carboxymethyl cellulose from sugar beet pulp cellulose and rheological behaviour of carboxymethyl cellulose. *Carbohydrate Polymers*, *54*, 73–82.

Uruş, S., Serindağ, O., & Diğrak, M. (2005). Synthesis, characterization, and antimicrobial activities of Cu(I), Ag(I), Au(I), and Co(II) complexes with $[CH_3N(CH_2PPh_2)_2]$. *Heteroatom Chemistry*, *16*(6), 484–491.

Vaca-Garcia, C., Borredon, M. E., & Gaseta, A. (2001). Determination of the degree of substitution (DS) of mixed cellulose esters by elemental analysis. *Cellulose*, *8*, 225–231.

Varshney, V. K., Gupta, P. K., Naithani, S., Khullar, R., Bhatt, A., & Soni, P. L. (2006). Carboxymethylation of α-cellulose isolated from Lantana camara with respect to degree of substitution and rheological behavior. *Carbohydrate Polymers*, *63*, 40–45.

Vilela, C., Freire, C. S. R., Marques, P. A. A. P., Trindade, T., Neto, C. P., & Fardim, P. (2010). Synthesis and characterization of new $CaCO_3$/cellulose nanocomposites prepared by controlled hydrolysis of dimethylcarbonate. *Carbohydrate Polymers*, *79*, 1150–1156.

Wada, M., Ike, M., & Tokuyasu, K. (2010). Enzymatic hydrolysis of cellulose I is greatly accelerated via its conversion to the cellulose II hydrate form. *Polymer Degradation and Stability*, *95*, 543–548.

Wang, X., Du, Y., & Liu, H. (2004). Preparation, characterization and antimicrobial activity of chitosan–Zn complex. *Carbohydrate Polymers*, *56*, 21–26.

Yang, S., Guo, Z., Zhou, Y., Zhou, L., Xue, Q., Miao, F., et al. (2010). Synthesis and moisture absorption and retention activities of a carboxymethyl and a quaternary ammonium derivative of α,α-trehalose. *Carbohydrate Research*, *345*, 120–123.

Yaşar, F., Toğrul, H., & Arslan, N. (2007). Flow properties of cellulose and carboxymethyl cellulose from orange peel. *Journal of Food Engineering*, *81*, 187–199.

Yeşilel, O. Z., & Ölmez, H. (2006). Spectrothermal studies of 1,10-phenanthroline complexes of Co(II), Ni(II), Cu(II) and Cd(II) orotates. *Journal of Thermal Analysis and Calorimetry*, *86*(1), 211–216.

Yeşilel, O. Z., Ölmez, H., & İçbudak, H. (2007). Orotic acid complexes of Co(II), Ni(II), Zn(II) and Cd(II) with imidazole syntheses, spectroscopic and thermal studies. *Journal of Thermal Analysis and Calorimetry*, *89*, 555–559.

Yuen, S.-N., Choi, S.-M., Phillips, D. L., & Maa, C.-Y. (2009). Raman and FTIR spectroscopic study of carboxymethylated non-starch polysaccharides. *Food Chemistry*, *114*, 1091–1098.

Zeleňák, V., Vargová, Z., & Györyová, K. (2007). Correlation of infrared spectra of zinc(II) carboxylates with their structures. *Spectrochimica Acta Part A*, *66*, 262–272.